Journal of Magnetic Resonance 230 (2013) 98–110

Contents lists available at SciVerse ScienceDirect

Journal of Magnetic Resonance

journal homepage: www.elsevier.com/locate/jmr

Direct observation of ^{17}O–$^{185/187}Re$ ^{1}J-coupling in perrhenates by solid-state ^{17}O VT MAS NMR: Temperature and self-decoupling effects

Hans J. Jakobsen [a,b,*], Henrik Bildsøe [a,b], Michael Brorson [c], Zhehong Gan [d], Ivan Hung [d]

[a] Danish Instrument Centre for Solid-State NMR Spectroscopy, Department of Chemistry, Aarhus University, DK-8000 Aarhus C, Denmark
[b] Interdisciplinary Nanoscience Center (iNANO), Department of Chemistry, Aarhus University, DK-8000 Aarhus C, Denmark
[c] Haldor Topsøe A/S, Nymøllevej 55, DK-2800 Lyngby, Denmark
[d] National High Magnetic Field Laboratory, 1860 East Paul Dirac Drive, Tallahassee, FL 32310, USA

ARTICLE INFO

Article history:
Received 14 September 2012
Revised 16 January 2013
Available online 9 February 2013

Keywords:
Solid-state ^{17}O VT MAS NMR
$KReO_4$ and NH_4ReO_4
Isotropic $^{1}J(^{17}O–^{187}Re)$ spin–spin coupling in solids
Theory
Spectral simulations
Dynamics
Relaxation times
Self-decoupling
Reduced $^{1}K(^{17}O–M)$ isotropic spin-spin couplings

ABSTRACT

^{17}O MAS NMR spectra recorded at 14.1 T and room temperature (RT) for ^{17}O-enriched samples of the two perrhenates, $KReO_4$ and NH_4ReO_4, exhibit very similar *overall* appearances of the manifold of spinning sidebands (ssbs) for the satellite transitions (STs) and the central transition (CT). These overall appearances of the spectra are easily simulated in terms of the usual quadrupole coupling and chemical shift interaction parameters. However, a detailed inspection of the line shapes for the individual ssbs of the STs and, in particular, for the CT in the spectrum of $KReO_4$ reveals line-shape features, which to our knowledge have not before been observed experimentally in 1D MAS NMR spectra for any quadrupolar nucleus, nor emerged from simulations for any combination of second-order quadrupolar interaction and chemical shift anisotropy. In contrast, such line-shape features are not observed for the corresponding ssbs (STs and CT) in the 14.1 T RT ^{17}O MAS NMR spectrum of NH_4ReO_4. Considering the additional interaction of a combination of residual heteronuclear ^{17}O–$^{185/187}Re$ dipolar and scalar J coupling between this spin pair of two quadrupolar nuclei, spectral simulations for $KReO_4$ show that these interactions are able to account for the observed line shapes, although the expected $^{1}J(^{17}O–^{185/187}Re)$ six-line spin–spin splittings are not resolved. Low-temperature, high-field (21.1 T) ^{17}O VT MAS NMR spectra of both $KReO_4$ and NH_4ReO_4 show that full resolution into six-line multiplets for the centerbands are achieved at −90 °C and −138 °C, respectively. This allows determination of $^{1}J(^{17}O–^{187}Re) = -268$ Hz and −278 Hz for $KReO_4$ and NH_4ReO_4, respectively, i.e., an isotropic ^{1}J coupling and its sign between two quadrupolar nuclei, observed for the first time directly from solid-state one-pulse 1D MAS NMR spectra, without resort to additional 1D or 2D experiments. Determination of $T_1(^{187}Re)$ spin–lattice relaxation times, observed indirectly through a 2D ^{17}O EXSY experiment for NH_4ReO_4 at several low temperatures, show that the dynamics observed for the ReO_4^- anion in the ^{17}O VT MAS NMR spectra at low temperatures are caused by self-decoupling of $^{1}J(^{17}O–^{187}Re)$. The $^{1}J(^{17}O–^{187}Re)$ values determined here for ReO_4^- from solid-state ^{17}O MAS NMR, along with literature $^{1}J(^{17}O–M)$ values for oxoanions (M being a quadrupolar nucleus) obtained from liquid-state NMR, have allowed correlations to be established between the reduced coupling constant $^{1}K(^{17}O–M) = 2\pi\ ^{1}J(^{17}O–M)/(\gamma_{^{17}O}\ \gamma_M\ h)$ and the atomic number of M.

1. Introduction

Recently we reported a variable-temperature (VT) ^{17}O MAS NMR investigation on the two alkali metal tungstates Cs_2WO_4 and K_2WO_4, in order to compare the determined ^{17}O solid-state NMR parameters for the tetraoxotungstate anions (WO_4^{2-}) [1] with the corresponding ^{33}S quadrupole coupling (C_Q and η_Q) and chemical shift (δ_σ, η_σ, and δ_{iso}) parameters for a series of WS_4^{2-} salts with different monovalent cations, determined earlier in our laboratory [2]. This comparison has allowed a complete assignment, not only for the different sets of ^{17}O and ^{33}S, but also for the ^{77}Se spectral parameters to the three crystallographically unique O-, S-, and Se-sites (e.g., S(1,1), S(2), and S(3)) reported for M_2WO_4, M_2WS_4, and $(NH_4)_2WSe_4$ [1]. Prompted by these observations, it was tempting to investigate whether correlations could be observed between the recently determined solid-state ^{33}S spectral parameters for a tetrathioperrhenate anion (ReS_4^-) [3], and the ^{17}O solid-state NMR anisotropic parameters for ordinary perrhenate anions (ReO_4^-), which to our knowledge have not yet been investigated.

Herein we report a ^{17}O MAS NMR study on the two perrhenates $KReO_4$ and NH_4ReO_4, performed at the two magnetic field

* Corresponding author at: Danish Instrument Centre for Solid-State NMR Spectroscopy, Department of Chemistry, Aarhus University, DK-8000 Aarhus C, Denmark. Fax: +45 8619 6199.
E-mail address: hja@chem.au.dk (H.J. Jakobsen).

1090-7807/$ - see front matter © 2013 Elsevier Inc. All rights reserved.
http://dx.doi.org/10.1016/j.jmr.2013.01.012

strengths of 14.1 T (81.34 MHz) and 21.1 T (121.50 MHz), in order to retrieve the ^{17}O anisotropic quadrupole coupling and chemical shift parameters for the perrhenate ReO_4^- anions in these two compounds, which have been extensively studied by X-ray/neutron diffraction [4–8], $^{185/187}Re$ NQR [9–12], ^1H NMR [13], and more recently also in some impressive studies (from two research groups) by solid-state $^{185/187}Re$ NMR spectroscopy [12,14]. The initial recording of the ^{17}O MAS NMR spectra at ambient/room temperature (RT) and 14.1 T for $KReO_4$ show some quite unexpected features for the line shapes within the individual spinning sidebands (ssbs) for the satellite transitions (STs) and the central transition (CT). To our knowledge such line shapes have not been observed earlier in 1D MAS NMR spectra for any quadrupolar nucleus. These line shapes are absent for the ssbs of the STs and CT in the RT spectrum of NH_4ReO_4, although the overall envelopes of the ssb manifold for the STs in $KReO_4$ and NH_4ReO_4 exhibit quite similar appearance. Bearing in mind the ^{17}O dynamics recently observed for the WO_4^{2-} oxoanion in the solid-state for Cs_2WO_4 from variable temperature (VT) ^{17}O MAS NMR experiments [1], it was subsequently decided to investigate if the different appearances for the RT ^{17}O MAS spectra of the two perrhenates could be explained by means of ^{17}O VT MAS experiments. However, before such VT experiments were performed, preliminary simulations concerned with reproducing the line-shape features for the individual ssbs in the RT ^{17}O MAS spectrum of $KReO_4$, indicated that these line shapes arise from a combination of residual heteronuclear ^{17}O–$^{185/187}Re$ dipolar and isotropic J couplings between spin pairs of two quadrupolar nuclei. Since the line shapes for the CT and ssbs of the STs are only partly resolved in the RT ^{17}O MAS spectrum at 14.1 T, a gain in resolution could be foreseen, if possible effects from molecular dynamics and $^{185/187}Re$- or ^{17}O-relaxation processes could be reduced, by recording ^{17}O MAS spectra for the two samples at low temperatures and high magnetic field. Because VT instrumentations for such experiments are not available at Aarhus University, these experiments have been performed on the 21.1 T spectrometer at the National High Magnetic Field Laboratory, Florida State University, Tallahassee.

During the past decade there have been numerous reports on the observation of J couplings in solid-state NMR between two spin-1/2 nuclei and, more importantly, between a spin $I = 1/2$ nucleus dipole-coupled to a neighboring quadrupolar nucleus $S \geqslant 1$, and usually observed in the spectrum of the spin $I = 1/2$ nucleus [15–20]. The exploratory study, on the observation of the latter type of splittings, dates back to the spin-pair $I = 1/2$, $S = 1$, as observed for the case of ^{13}C–^{14}N in the ^{13}C MAS NMR spectra for the amide bond of ^{14}N-containing biomolecules [21] and polymers [22]. Reports on direct NMR detection and analysis of such dipolar- and J-coupling effects between two quadrupolar nuclei in the solid-state are scarce [19,23], most likely because these small dipolar- and J-coupling interactions are masked by the dominating quadrupole effects for either of the observed quadrupolar nuclei. Recently Wi and Frydman [24] presented a theoretical and numerical analysis for such dipole/J-coupling interactions between two quadrupolar nuclei with particular attention being paid to the, at that time, quite new high-resolution techniques such as multiple-quantum MAS (MQMAS) [25], dynamic-angle spinning (DAS) [26], and double-rotation (DOR) [27] NMR experiments for studying half-integer quadrupolar nuclei in solids. In addition these authors [24] presented MQMAS results for ^{11}B–^{14}N, ^{11}B–^{11}B, and ^{55}Mn–^{55}Mn spin pairs, which validate their theoretical predictions and determinations of J couplings from optimized fitting to the experimental 2D MQMAS line shapes of their spectra. This procedure allowed the following isotropic J couplings to be determined from 2D optimized fits to the experimental MQMAS spectra for their compounds: $^1J(^{11}B$–$^{14}N) = 20 \pm 10$ Hz for a trimethylamine borane complex, $^1J(^{11}B$–$^{11}B) = 85 \pm 20$ Hz for the bispinacolato borane compound, and $^1J(^{55}Mn$–$^{55}Mn) = 65 \pm 5$ Hz for dimanganese decacarbonyl [24]. Following this investigation two other small J couplings between two quadrupolar nuclei of low atomic number M have to our knowledge been determined in solids employing a combination of different solid-state NMR experiments, i.e., $^2J(^{17}O$–$^{17}O) = -4.5 \pm 0.9$ Hz for glycine·^{2}HCl [28] and $^1J(^{11}B$–$^{35}Cl) = -30 \pm 15$ Hz for B-chlorocatecholborane [29], although evidence for $^1J(^{11}B$–$^{75}As)$ in borane triphenylarsine [30] and $^1J(^{17}O$–$^{27}Al)$ in calcium aluminates [31] have also been reported.

In the present study we succeeded in resolving a much larger isotropic J coupling between two quadrupolar nuclei in solid-state NMR, i.e., $^1J(^{17}O$–$^{185/187}Re)$ for the ReO_4^- anion in both $KReO_4$ and NH_4ReO_4 directly from ordinary one-pulse low-temperature 1D ^{17}O MAS NMR experiments (down to −138 °C). We also note that Re has by far the highest atomic number, M(Re) = 75, for one of the nuclei in the spin pair of quadrupoles, where such J couplings have been determined. Based on the theoretical equations outlined in the study by Wi and Frydman [24], we have incorporated the additional residual dipole/J-coupling terms into an expanded version of the STARS simulation/fitting program, which thus allows optimized fits, for all obtained experimental ^{17}O VT MAS NMR spectra, to be performed. The effect of molecular dynamics on the appearances of the spectra has been probed by $T_2(^{17}O)$ spin-echo measurements at two quite different low temperatures. In addition, the resolved J couplings allow for indirect VT measurements of the $T_1(^{185/187}Re)$ relaxation times, which could also affect the appearance of the ^{17}O MAS spectra. The $T_1(^{185/187}Re)$ relaxation times are difficult to measure directly due to the extremely broad static $^{185/187}Re$ powder spectra [12,14], and have to our knowledge not been determined until now.

Finally, we mention that isotropic J couplings between two quadrupolar nuclei have in several cases been observed for $^1J(^{17}O$–M) in solution-state NMR of oxoanions MO_4^{n-} (M = ^{51}V, ^{53}Cr, ^{55}Mn, ^{95}Mo, and ^{99}Tc) [32–34], but to our knowledge not for such spin pairs in solid-state NMR. For example, an aqueous solution of ^{17}O-enriched $KMnO_4$ exhibits a six-line splitting pattern in its ^{17}O NMR spectrum [33], while its solid-state ^{17}O MAS NMR spectrum consists of a quite narrow singlet [35]. The abovementioned solution-state studies hold for M possessing a rather low atomic number and the most recent study [34] has called for determination of $^1J(^{17}O$–M) for much higher M-atomic numbers in order to confirm a proposed correlation between the *reduced* coupling constant $^1K(^{17}O$–M$) = 2\pi\ ^1J(^{17}O$–M$)/(\gamma_{^{17}O}\ \gamma_M\ \hbar)$ and the atomic number for M [34]. The highest atomic number for a reported $^1J(^{17}O$–M) is for ^{99}Tc (M = 43, spin $I = 9/2$) in the TcO_4^- anion of NH_4TcO_4, where $^1J(^{17}O$–$^{99}Tc) = 131.6$ Hz is obtained from its solution-state 10-line ^{17}O NMR spectrum [34]. This note [34] also reports that no accurate coupling constants are available for ReO_4^- and WO_4^{2-} (i.e., for ReO_4^- in agreement with ^{17}O and ^{187}Re NMR spectra of an aqueous solution recorded for our sample for NH_4ReO_4 which both show a single Lorentzian line with FWHM = 110 Hz and 11.1 kHz, respectively). In addition, the results obtained by Bank and Schwenk [36] from a solution-state ^{17}O NMR study of a 35% ^{17}O-enriched $H_2{}^{17}O$ solution of Na_2WO_4, which show that $|^1J(^{17}O$–$^{183}W)| < 10$ Hz, have suggested [34] that $^1K(^{17}O$–$^{183}W)$ in WO_4^{2-} (^{183}W, spin $I = 1/2$) may contradict the observed trend for $^1K(^{17}O$–M). Thus, it is fortunate that the present investigation has been successful in resolving $^1J(^{17}O$–$^{185/187}Re)$ from solid-state NMR, which at least for the ReO_4^- anion confirms an extension of the proposed correlation of $^1K(^{17}O$–M) with the atomic number M for higher M values. Moreover, the present work would indicate that it may be possible to determine a value for $^1J(^{17}O$–$^{183}W) \sim 280$ Hz in the WO_4^{2-} anion from solid-state ^{17}O or ^{183}W VT MAS NMR investigations (*vide infra*).

2. Experimental

2.1. Materials and ^{17}O-enrichment

Ammonium perrhenate was a sample from Molibdenos Y Metales S.A., Chile, and was used without further purification for the ^{17}O-enrichment. Potassium perrhenate was prepared from this raw material by the following procedure where Schlenk techniques (N_2) were used to prevent potential contamination of the product by carbonate due to CO_2 absorption from the ambient air: 5.36 g NH_4ReO_4 was dissolved in 90 ml of mildly heated water. A solution of 2.64 g KOH (85%) in a small amount of water was added causing a white precipitate to form. The basic suspension was then treated with a bubbling flow of N_2 for 3 h while being held close to boiling point in order to remove all ammonia and ammonium. In the cause of this purge, a clear solution was obtained at one point in time but later partial precipitation occurred. After removal of more solvent, the white product was isolated and washed three times with ethanol, dried 24 h at 110 °C, and characterized as pure $KReO_4$ by powder X-ray diffraction. ^{17}O-enriched specimens of the two materials were obtained according to an earlier, almost 30-year old, procedure reported for incorporation of ^{17}O into tetrahedral MO_4^{n-} oxoanions (i.e., ^{17}O-exchange in a sealed glass ampoule containing a 40% ^{17}O-enriched $H_2{}^{17}O$ solution at 80 °C for 7 days) [35], however, for our purpose using only 10% $H_2{}^{17}O$, purchased from CortecNet, France.

2.2. Solid-state ^{17}O MAS NMR spectra

^{17}O RT MAS NMR experiments for $KReO_4$ and NH_4ReO_4 were performed at Aarhus University on a Varian Direct-Drive VNMRS-600 spectrometer (14.1 T) at 81.34 MHz, and at higher field and for VT MAS on a Bruker 900 MHz (21.1 T) Avance spectrometer at a frequency of 121.50 MHz at the National High Magnetic Field Lab (NHMFL), Florida State University (FSU), Tallahassee.

2.2.1. Varian Direct-Drive VNMRS-600 spectrometer

The initial ^{17}O MAS NMR experiments were performed on the Varian Direct-Drive VNMRS-600 spectrometer, equipped with an Oxford Instruments 14.1 T wide-bore magnet, and employed a Varian/Chemagnetics triple-resonance T3® MAS probe for 4.0 mm o.d. (82 μl sample volume) rotors. The magic angle of $\theta = 54.736°$ was adjusted to the highest possible precision ($\Delta\theta < \pm 0.005°$) by ^{14}N MAS NMR at 43.34 MHz using a sample of $NH_4H_2PO_4$ as recently described [37]. The two ^{17}O-enriched samples of $KReO_4$ and NH_4ReO_4 were both spun at a MAS frequency of $\nu_r = 6000$ Hz with a precision $\Delta\nu_r < 1.0$ Hz in ν_r, employing the experimental setup combined with a Varian/Chemagnetics MAS-speed controller, as recently described [38]. ^{17}O rf field strengths were calibrated using a sample of 10% $H_2{}^{17}O$, contained in a sealed glass tube, which also served as external reference. A 90° flip angle of $pw(90)_{liquid} = 6.5$ μs was obtained for the 10% $H_2{}^{17}O$ solution. Thus, the actual value of 2.0 μs employed for the solid-state ^{17}O MAS experiments corresponds to a liquid flip angle of 28° (or a 83° solids flip angle), which was used along with a relaxation delay of 30 s. For the ^{17}O MAS spectra we acquired 4000 and 5824 scans for the $KReO_4$ and NH_4ReO_4 sample, respectively, corresponding to total experimental times of about 33 and 48 h.

2.2.2. Bruker Avance-900 wide-bore 21.15 T spectrometer

High-field, low- and high-temperature ^{17}O MAS NMR spectra for the ^{17}O-enriched $KReO_4$ and NH_4ReO_4 samples were acquired on the 21.1 T wide-bore (105 mm i.d.) magnet, designed and constructed at the NHMFL, and equipped with a 900 MHz Bruker Avance console. The experiments employed a wide-bore (89 mm o.d.) variable-temperature (VT) broadband 3.2 mm double-resonance (^1H–X) MAS probe, also designed and built at the NHMFL. ^1H decoupling was not used for NH_4ReO_4 since spectra acquired at RT (23 °C) with and without ^1H decoupling showed identical line shape and line width for the centerband (FWHM ~1400 Hz). A 90° flip-angle $pw(90)_{liquid} = 5.0$ μs was obtained for the ^{17}O resonance of ordinary H_2O while a value of pw = 1.2 μs, which corresponds to a liquid 22° flip-angle (or a solids 65° flip angle) for the rf field strength of 50 kHz, was used for the MAS experiments. Although the $T_1(^{17}O)$ relaxation times for the two perrhenates were not determined, it soon became clear that of the two, $T_1(^{17}O)$ is very much longer for $KReO_4$ at all temperatures and that $T_1(^{17}O)$ increases dramatically for both $KReO_4$ and NH_4ReO_4 with decreasing temperatures. Also, we note that the NH_4^+ ions in NH_4ReO_4 (and most likely also the ReO_4^- ions) undergo rapid rotations [13], which averages the dipolar couplings from the protons and also causes a short $T_1(^{17}O)$. Such a relaxation mechanism is absent in $KReO_4$, resulting in its longer $T_1(^{17}O)$. Thus, relaxation delays were varied between 30 and 15 s for $KReO_4$ and between 10 and 1 s for NH_4ReO_4, where the longer delays were applied when approaching the lowest temperature (−138 °C), while the shorter delays were used at the higher temperatures (from RT up to ~70 °C) for both samples. Between about 890 and 100 scans (i.e., corresponding to total experimental times of about 7 h 25 min and 15 min, respectively) were acquired, depending on the signal-to-noise ratio required for the individual spectra. The MAS speed was not regulated, however, XSTARS optimizations (*vide infra*) revealed that the variation $\Delta\nu_r$ in spinning frequency is within $\Delta\nu_r < \pm 2$ Hz for $\nu_r \sim 12$ kHz for all spectra acquired. Because the actual temperature of the samples is highly dependent on the MAS-stator/VT design, the flow rates of both the VT- and air-bearing/drive-gasses and their temperatures, and finally the MAS rotor ν_r frequency (frictional heating [39]), the sample temperatures for the different Bruker VT (BTV) set-temperatures for the sample cooling or heating gas have been calibrated for $\nu_r = 12$ kHz using the standard procedure for a sample of $Pb(NO_3)_2$ [40]. Since the adjustment of the magic-angle setting will most likely change slightly when going from RT to the lowest temperatures (−138 °C) required for our experiments, the magic angle $\theta = 54.736°$ was adjusted at these two temperatures to the highest possible precision ($\Delta\theta < \pm 0.003°$) by ^{23}Na MAS NMR using a sample of $NaNO_3$ at 237.60 MHz as described elsewhere [41].

Indirect VT $T_1(^{185/187}Re)$ relaxation time measurements were carried out using a ^{17}O three-pulse 2D-NOESY type sequence [42]. The rf carrier was set in the center of the *J*-multiplet pattern and the value t_1 between the first two pulses was fixed at values in the range 410–450 μs, depending on the width of the multiplet. The phase cycling of the two pulses and the receiver selects the sine component corresponding to I_xS_z coherence. The $T_1(^{185/187}Re)$ relaxation leads to decay for the anti-phase coherence as a function of the mixing time t_{mix}, which allows for its measurement. This kind of pulse sequence has earlier been used for spin-diffusion measurements under rotational-resonance conditions [43].

2.3. Simulation software and spectral analysis

A computer program based on average Hamiltonian theory has been developed in order to simulate and/or fit the solid-state MAS NMR spectrum of a quadrupole nucleus for a heteronuclear *I*–*S* spin-pair of quadrupolar nuclei, which exhibit the mutual interactions of direct (dipole-*D*) and indirect (isotropic-*J* + anisotropic-δ_J) spin–spin coupling in addition to the usual quadrupole coupling and chemical shift interactions. A solution to this problem has earlier been addressed by Wi and Frydman [24], and their theoretical derivations are here adapted to the conventions used in the STARS software package [44–46], resulting in the new simulation/fitting

software used here and dubbed XSTARS. This gives the following expressions (in addition to the isotropic chemical shift and isotropic J spin–spin coupling terms) for the 1st and 2nd order terms relevant for observation of the spin I transitions:

$$h^{-1}H_{\sigma}^{(1)} = \frac{2}{\sqrt{6}}R_{20}^{\sigma}I_z \tag{1}$$

$$h^{-1}H_{D'}^{(1)} = \frac{2}{\sqrt{6}}R_{20}^{D'}I_zS_z \tag{2}$$

$$h^{-1}H_{Q_I}^{(1)} = \frac{1}{\sqrt{6}}(3I_z^2 - I(I+1))R_{20}^{Q_I} \tag{3}$$

$$h^{-1}H_{\sigma Q_I}^{2} = -\frac{1}{2\upsilon_{0,I}}(3I_z^2 - I(I+1))\left(R_{21}^{Q_I}R_{2-1}^{\sigma} + R_{2-1}^{Q_I}R_{21}^{\sigma}\right) \tag{4}$$

$$\begin{aligned} h^{-1}H_{D'Q}^{(2)} = &-\frac{3S_z^2 - S(S+1)}{2\upsilon_{0,S}}I_z\left(R_{2-1}^{D'}R_{21}^{Q_S} + R_{21}^{D'}R_{2-1}^{Q_S}\right) \\ &-\frac{3I_z^2 - I(I+1)}{2\upsilon_{0,I}}S_z\left(R_{2-1}^{D'}R_{21}^{Q_I} + R_{21}^{D'}R_{2-1}^{Q_I}\right) \end{aligned} \tag{5}$$

$$\begin{aligned} h^{-1}H_{Q_IQ_I}^{(2)} = &-\frac{(I_z - 4I_zI(I+1) + 8I_z^3)}{2\upsilon_{0,I}}R_{2-1}^{Q_I}R_{21}^{Q_I} \\ &-\frac{(I_z - 2I_zI(I+1) + 2I_z^3)}{2\upsilon_{0,I}}R_{2-2}^{Q_I}R_{22}^{Q_I} \end{aligned} \tag{6}$$

It is noted that the anisotropic J coupling term (δ_J) is included in the D' term ($D' = D + \delta_J$, *vide infra*). In view of the large ^{187}Re quadrupole coupling constants for the $KReO_4$ sample, $C_Q(^{187}Re) = 178.8$, 184.1, and 185.6 MHz at 23, −125, and −196 °C, respectively, as calculated from the earlier determined NQR frequencies [9] (and therefore an even slightly larger average $C_Q(^{185}Re)$ ~192 MHz across this temperature range), we have also included two 3rd order cross-terms $H_{D'QQ}$ and H_{JQQ}:

$$\begin{aligned} h^{-1}H_{D'QQ}^{(3)} = &\frac{2}{\sqrt{6}\upsilon_{0,S}^2}(S_z - 4S_zS(S+1) + 8S_z^3)I_zR_{20}^{D'}R_{21}^{Q_S}R_{2-1}^{Q_S} \\ &+\frac{2}{\sqrt{6}\upsilon_{0,S}^2}(S_z - 2S_zS(S+1) + 2S_z^3)I_zR_{20}^{D'}R_{22}^{Q_S}R_{2-2}^{Q_S} \\ &+\frac{3}{\sqrt{6}\upsilon_{0,S}^2}(S_z - 4S_zS(S+1) + 8S_z^3)I_z(R_{21}^{D'}R_{2-1}^{Q_S}R_{20}^{Q_S} \\ &+R_{2-1}^{D'}R_{21}^{Q_S}R_{20}^{Q_S}) + \frac{1}{\upsilon_{0,S}^2}(S_z - 3S_zS(S+1) \\ &+5S_z^3)I_z(R_{21}^{D'}R_{21}^{Q_S}R_{2-2}^{Q_S} + R_{2-1}^{D'}R_{2-1}^{Q_S}R_{22}^{Q_S}) \end{aligned} \tag{7}$$

$$\begin{aligned} h^{-1}H_{JQQ}^{(3)} = &\frac{1}{\upsilon_{0,S}^2}(S_z - 4S_zS(S+1) + 8S_z^3)I_zJ_{iso}R_{21}^{Q_S}R_{2-1}^{Q_S} + \frac{1}{\upsilon_{0.S}^2}(S_z \\ &-2S_zS(S+1) + 2S_z^3)I_zJ_{iso}R_{22}^{Q_S}R_{2-2}^{Q_S} \end{aligned} \tag{8}$$

R_{lm}^{λ} are geometrical factors for the interactions in the laboratory frame derived from their principal values. The description in the principal axis system (PAS^{λ}) for the various interactions is first transformed to a common molecular system using Euler rotations $\alpha^{\lambda}(z)$ followed by $\beta^{\lambda}(y')$ and $\gamma^{\lambda}(z'')$, next to the rotor frame, and finally to the laboratory frame. In the PAS systems the geometrical factors are:

$$R_{20}^{\sigma,PAS} = -\frac{\sqrt{6}}{2}\gamma_I B_0\delta_{\sigma} \quad R_{2\pm1}^{\sigma,PAS} = 0 \quad R_{2\pm2}^{\sigma,PAS} = -\frac{1}{2}\gamma_I B_0\delta_{\sigma}\eta_{\sigma} \tag{9}$$

$$R_{20}^{D',PAS} = -\sqrt{6}D' \quad R_{2\pm1}^{D',PAS} = 0 \quad R_{2\pm2}^{D',PAS} = 0 \tag{10}$$

$$\begin{aligned} R_{20}^{Q_X,PAS} &= \sqrt{6}\frac{C_{Q_X}}{4X(2X-1)} \quad R_{2\pm1}^{Q_X,PAS} = 0 \quad R_{2\pm2}^{Q_X,PAS} \\ &= -\frac{C_{Q_X}\eta_{Q_X}}{4X(2X-1)} \end{aligned} \tag{11}$$

For the quadrupole coupling and chemical shift parameters we use the standard conventions from STARS [44–46]:

$$C_{Q_X} = \frac{eQ_X}{h}V_{zz}^X \quad \eta_{Q_X} = \frac{(V_{yy}^X - V_{xx}^X)}{V_{zz}^X}, \quad X = I,S \tag{12}$$

and

$$\delta_{\sigma} = \delta_{iso} - \delta_{zz} \quad \eta_{\sigma} = \frac{(\delta_{xx} - \delta_{yy})}{\delta_{\sigma}} \tag{13}$$

where δ_{xx}, δ_{yy}, δ_{zz}, δ_{iso} correspond to the parameters – σ_{xx}, – σ_{yy}, – σ_{zz}, – σ_{iso}. $D' = D + \delta_J$ is the sum of the dipole coupling ($D = (\gamma_I\gamma_S\mu_0\hbar)(8\pi^2r_{IS}^3)^{-1}$ Hz) and the anisotropy δ_J of the J coupling ($\delta_J = 2/3(J_{||} - J_{\perp})$), where it is assumed that the tensors for the direct dipole and indirect spin–spin coupling interactions are coincident. Finally, we note the usage of the convention

$$\left|\lambda_{zz} - \frac{1}{3}Tr(\lambda)\right| \geqslant \left|\lambda_{xx} - \frac{1}{3}Tr(\lambda)\right| \geqslant \left|\lambda_{yy} - \frac{1}{3}Tr(\lambda)\right| \tag{14}$$

for the principal elements ($\lambda_{\alpha\alpha} = V_{\alpha\alpha}$, $\delta_{\alpha\alpha}$) of the tensors.

In the equations above we use $\nu_{0,X} = -\gamma_X B_0/2\pi$, $X = I, S$, and since ^{17}O has a negative gyromagnetic ratio the transition frequencies are obtained as $\nu = (E_m - E_{m-1})h^{-1}$. The molecular frame system has been selected with its z-axis along the Re–^{17}O interatomic vector and with the Re quadrupole principal z-axis in the zx-plane of the molecular frame. It is noted that the near tetrahedral geometry of the ReO_4^- cation makes the angle between the two PAS z-axis for Q(Re) and D' very close to the magic angle, thereby making the second- and third-order terms, $H_{D'Q}^{(2)}$ and $H_{D'QQ}^{(3)}$, very small. The values for $\beta(Q(Re))$ and the Re quadrupole coupling constant have accordingly been fixed during all optimizations. The contribution to the natural line width, caused by dynamics/relaxation, is simulated by a Lorentzian line shape identical for all Re manifolds and ssbs in combination with a Gaussian line broadening, specific for each Re manifold of ssbs. The Gaussian broadening is assumed to be identical for manifolds, which have the same numerical value for m_Z(Re). Although the experimental spectra represent overlap of spectra for the two $^{185/187}$Re isotopes, the simulations were performed for the ^{187}Re isotope only, since simulations for each of the two isotopes show that, for all practical purposes, identical ^{17}O MAS NMR spectra are obtained employing the parameters relevant for the ^{17}O spin systems studied here for $KReO_4$ and NH_4ReO_4.

3. Results

Before presenting the experimental ^{17}O results of the present study, we first briefly reiterate the properties for the observed half-integer ^{17}O quadrupole nucleus: spin $I = 5/2$, $\gamma(^{17}O) = -3.628 \times 10^7$ rad T^{-1} s^{-2}, 0.037% natural abundance, and quadrupole moment $Q(^{17}O) = -0.026$ barn; however, implemented here with an ^{17}O-enrichment for the two samples as described above. In addition to the ^{17}O nucleus, the properties of the two rhenium half-integer quadrupolar nuclei ^{185}Re and ^{187}Re (both spin $I = 5/2$) play an important role in the interpretation of the ^{17}O MAS NMR spectra. ^{185}Re (37.07% natural abundance, $\gamma(^{185}Re) = 6.1057 \times 10^7$ rad T^{-1} s^{-1}, $Q(^{185}Re) = 2.4$ barn) and ^{187}Re (62.93% natural abundance, $\gamma(^{187}Re) = 6.1682 \times 10^7$ rad T^{-1} s^{-1}, $Q(^{187}Re) = 2.2$ barn) constitute a total of 100% of the rhenium–^{17}O coupling interactions and therefore, should potentially be easily

retrieved from the ^{17}O MAS line shapes. Moreover, since the ratio $\gamma(^{187}Re)/\gamma(^{185}Re) = 1.0102$, the pair of $J(^{17}O–^{185}Re)$ and $J(^{17}O–^{187}Re)$ scalar couplings should differ by only a few Hz (~3 Hz for the present results, *vide infra*), and therefore would be indiscernible from the ^{17}O MAS NMR spectra, even without being masked by second-order ^{17}O quadrupolar line broadening, molecular dynamics, and/or relaxation effects. This statement also holds for the pair of $D(^{17}O–^{185}Re)$ and $D(^{17}O–^{187}Re)$ dipolar couplings. Finally, the very large and quite similar quadrupole moments, $Q(^{185}Re)$ and $Q(^{187}Re)$, for both rhenium spin isotopes lead to very large and, most importantly, fairly similar magnitudes for the quadrupole coupling constants, $C_Q(^{185}Re)$ and $C_Q(^{187}Re)$, in the same compound. These properties justify our abovementioned observation (see Section 2.3), that the simulations need only be performed, taking one of the rhenium isotopes into account, of which we have chosen the most abundant, i.e. ^{187}Re.

3.1. 14.1 T RT ^{17}O MAS NMR on the Varian Direct-Drive spectrometer

The first ^{17}O MAS NMR spectra obtained for the two perrhenates are the RT spectra of $KReO_4$ and NH_4ReO_4 acquired at Aarhus University on a 14.1 T Varian Direct-Drive spectrometer.

3.2. $KReO_4$

Experimental ^{17}O MAS NMR spectra for $KReO_4$ are shown in the upper row of Fig. 1, while the corresponding optimized-fitted (XSTARS) simulated spectra are illustrated in the lower row. Fig. 1a shows the full experimental spectrum (STs and CT) with the complete envelope of ssbs for all satellite transitions (STs), and with a cut-off height at 1/10 of the maximum height for the central transion (CT) centerband. In Fig. 1b an expansion of the region for the CT centerband with a few ssbs from the full experimental spectrum in Fig. 1a is presented. The line shapes observed for the centerband and ssbs in Fig. 1b appear quite unusual and cannot be reproduced using any of the standard software packages (e.g., STARS [44–46] or WSolids1 [47]) developed for the simulation of second- or higher-order quadrupolar line shapes in MAS NMR spectra of half-integer quadrupolar nuclei. For this reason we extended the STARS program to include the combination of residual heteronuclear dipolar and indirect *J* coupling between two quadrupolar nuclei (i.e., XSTARS, *vide supra*). Using XSTARS, the final optimized/simulated spectrum obtained for the full experimental spectrum in Fig. 1a, including the complete manifold of ssbs, is displayed in Fig. 1c. An expansion of the full simulated spectrum in Fig. 1c for the CT and a few of the ssbs in the CT region is shown in Fig. 1d. Excellent agreements between the experimental and fitted spectra are observed for the 14.1 T RT spectra of $KReO_4$ in Fig. 1. To further illustrate the excellent agreements obtained for the individual line shapes of the ssbs in the experimental and simulated spectra in Fig. 1, expansions of selected regions with quite different ssb line shapes in the experimental and fitted spectra for $KReO_4$ in Fig. 1 are illustrated in Fig. 2a and b, respectively. The impressive fits between the experimental and fitted spectra in Figs. 1 and 2 illustrate that optimum performance has been achieved for both the 14.1 T RT experiment and XSTARS software. The final spectral parameters obtained from the XSTARS fit to the ^{17}O RT MAS NMR spectrum of $KReO_4$ at 14.1 T are summarized in the first row of Table 1a and 1b.

3.3. NH_4ReO_4

The experimental 14.1 T RT ^{17}O MAS NMR spectrum, including both the CT and STs, for the sample of NH_4ReO_4 is shown in Fig. 3a. Although the overall envelope for the manifold of ssbs in

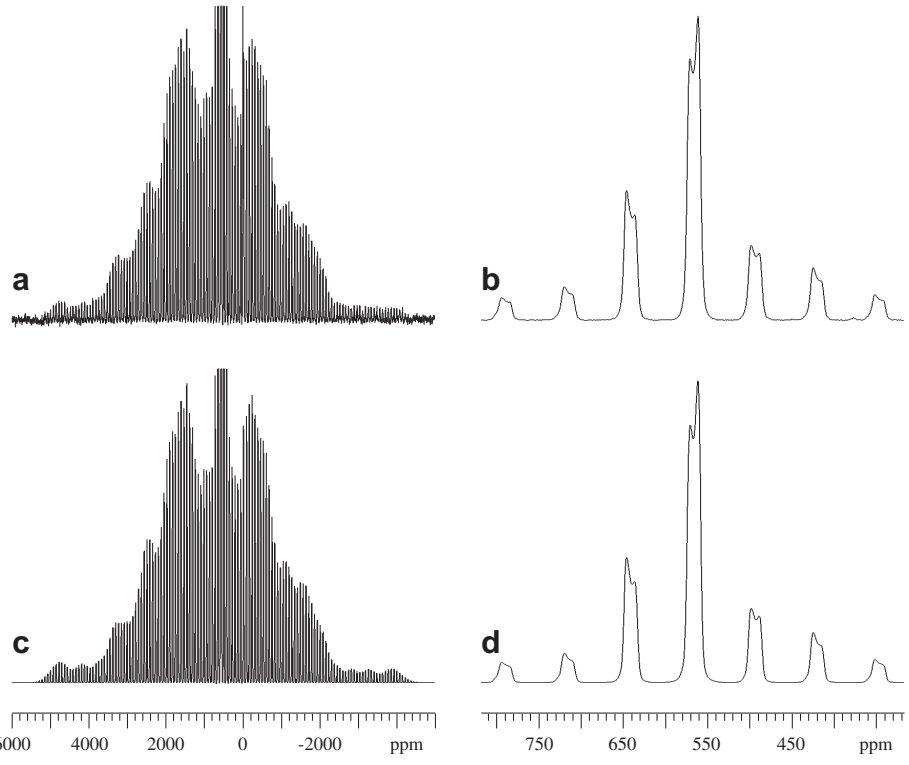

Fig. 1. 81.34 MHz (14.1 T) ^{17}O MAS NMR spectra of the ^{17}O-enriched sample of $KReO_4$, $\nu_r = 6000$ Hz, and at RT (23 °C). (a) Experimental spectrum (4000 scans in 18 h) showing the complete manifold of spinning sidebands (ssbs) for a vertical expansion with a cut-off at 1/10 of the height for the centerband. We note that the narrow singlet ^{17}O resonance at 0 ppm originates from a minute amount of $H_2{}^{17}O$, which has been very difficult to completely remove immediately following the ^{17}O-enrichment procedure and drying of the sample. (b) Horizontal expansion of the experimental spectrum in (a) for the centerband region and a few of its ssbs, which illustrates the observed and unexpected line shapes. (c and d) Fitted (XSTARS), simulated spectra corresponding to the spectra in (a and b). The optimized XSTARS parameters are listed in Tables 1a and 1b for a deviation from exact magic-angle setting of $\Delta\theta = -0.007°$.

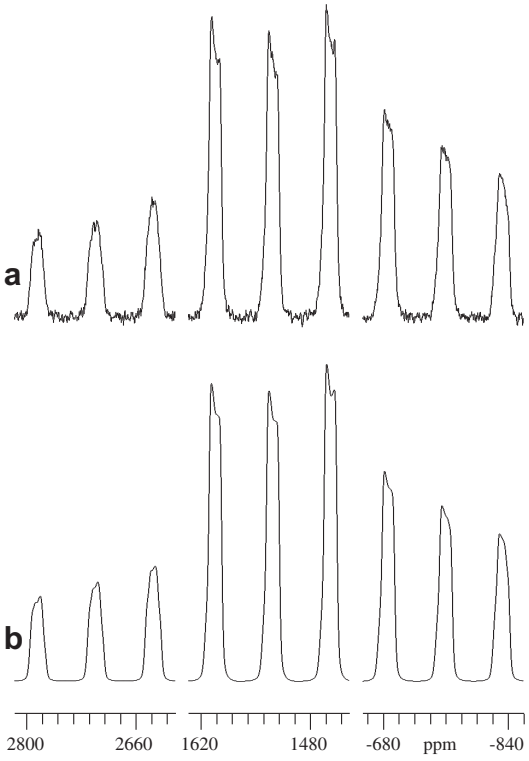

Fig. 2. Horizontal expansions for the ssbs in the experimental spectrum of $KReO_4$ in Fig. 1a is shown in (a) for three selected regions of the ssbs to illustrate their unexpected line shapes. (b) Expansions of the corresponding regions for the optimized simulated spectrum shown in Fig. 1c.

the ST spectrum of NH_4ReO_4 (Fig. 3a) displays a quite similar appearance to that observed for the ssbs in Fig. 1a for the ^{17}O MAS spectrum of $KReO_4$, the individual ssbs in the spectrum of NH_4ReO_4 appear without any line shape, however excessively broadened (FWHM ~ 1400 Hz), as illustrated by the expansion for the centerband region in Fig. 3b. To obtain an optimized fit and simulated spectrum for the experimental spectrum of NH_4ReO_4 (Fig. 3a), the new XSTARS software has been employed with values $D = 0$ for the heteronuclear dipolar coupling and $J = 0$ for the isotropic J coupling. For these values XSTARS becomes identical to STARS. The optimized simulated spectrum shows excellent agreements with respect to the experimental spectrum for both the full ssb envelope (Fig. 3a) and line shape for the ssbs (Fig. 3b), as illustrated by the corresponding simulated spectrum in Fig. 3c and for its expansion of the CT region in Fig. 3d. The final spectral parameters obtained from the XSTARS fit to the ^{17}O RT MAS NMR spectrum of NH_4ReO_4 at 14.1 T are summarized in the second row of Tables 1a and 1b. Because of the above observations at 14.1 T and RT, we became suspicious that effects of molecular dynamics, which we recently observed for the ^{17}O MAS NMR spectra of Cs_2WO_4 [1], could also be an issue in explaining the difference between the appearances for the ^{17}O MAS spectra of $KReO_4$ and NH_4ReO_4. This suggested the high-field 21.1 T VT ^{17}O MAS NMR investigation to be discussed below.

Table 1b
Optimized Euler angles describing the orientation for the ^{17}O quadrupole coupling ($\alpha(Q)$, $\beta(Q)$, $\gamma(Q)$) and chemical shift anisotropy ($\alpha(\delta_\sigma)$, $\beta(\delta_\sigma)$, $\gamma(\delta_\sigma)$) Principal Axis Systems (PAS) relative to the definition of a molecular frame system from ^{17}O VT MAS NMR spectra of $KReO_4$ and NH_4ReO_4[a,b].

Sample Experiment	Temp. (°C)	$\beta(Q)$	$\beta(\delta_\sigma)$
$KReO_4$/14.1 T	23, RT	9°	12°
NH_4ReO_4/14.1 T	23, RT	–	–
$KReO_4$/21.2 T	0	3°	22°
$KReO_4$/21.2 T	−16	−1°	15°
$KReO_4$/21.2 T	−90	6°	21°
NH_4ReO_4/21.2 T	−59	13°	13°
NH_4ReO_4/21.2 T	−90	21°	17°
NH_4ReO_4/21.2 T	−138	11°	−1°

[a] The Euler angles describe the orientation of the two PAS relative to a molecular frame system, which has been selected with its z-axis along the Re–^{17}O interatomic vector and with the Re quadrupole principal z-axis in the zx-plane of the molecular frame. Thus, the orientation of the Re quadrupolar PAS is given by the three angles (0,55,0), while the D' dipolar PAS is given by the three angles (0,0,0).

[b] We note that the two sets of Euler angles ($\alpha(Q)$, $\gamma(Q)$) and ($\alpha(\delta_\sigma)$, $\gamma(\delta_\sigma)$) have been shown both to be very insensitive towards an optimized fit of the experimental spectra compared to the otherwise optimized parameters used in the fitting process and listed in Table 1a. Thus, these two sets of parameters have been fixed to values of zero during the course of the fitting procedure. The error limits for the quite sensitive Euler angles $\beta(Q)$ and $\beta(\delta_\sigma)$ are both within ±5°.

3.4. 21.1 T VT ^{17}O MAS NMR on the Bruker Avance-900 spectrometer; $KReO_4$ and NH_4ReO_4 in general

While the high-field 21.1 T RT (23 °C) ^{17}O MAS NMR spectra of $KReO_4$ and NH_4ReO_4 exhibit line shapes for their respective centerbands, which are identical to the 14.1 T RT spectra in Figs. 1b and 3b, respectively, the intensity distributions of the ssbs within the manifold for the STs are different. The latter observation is obviously caused by the increased influence of the CSA contribution

Table 1a
^{17}O Quadrupole coupling (C_Q, η_Q), chemical shift parameters (δ_σ, η_σ, δ_{iso}), direct dipolar $D'(^{17}O–^{187}Re) = D + \delta_J$ coupling, isotropic $J = {}^1J(^{17}O–^{187}Re)$ coupling and its anisotropy δ_J, determined from ^{17}O VT MAS NMR spectra of $KReO_4$ and NH_4ReO_4 (see text).[a]

Sample Experiment	Temp. (°C)	C_Q (MHz)	η_Q	δ_σ (ppm)	η_σ	δ_{iso} (ppm)	J [b] (Hz)	D' (Hz)	δ_J (Hz)
$KReO_4$/14.1 T	23, RT	1.28	0.25	137	0.07	568	−224	−401	325
NH_4ReO_4/14.1 T	23, RT	1.25	0.16	133	0.02	567	–	–	–
$KReO_4$/21.2 T	0	1.30	0.25	144	0.40	569	−232	−493	233
$KReO_4$/21.2 T	−16	1.31	0.26	147	0.41	568	−238	−610	116
$KReO_4$/21.2 T	−90	1.34	0.26	150	0.43	568	−267	−594	103
NH_4ReO_4/21.2 T	−59	1.32	0.18	146	0.13	567	−228	−458	239
NH_4ReO_4/21.2 T	−90	1.36	0.20	151	0.01	567	−235	−427	270
NH_4ReO_4/21.2 T	−138	1.39	0.21	152	0.29	567	−278	−409	288

[a] The relevant Euler angles obtained from the optimizations for the fits of the experimental spectra are shown in Table 1b. The δ_{iso} values (relative to $H_2{}^{17}O$) have an error limit of ±0.5 ppm. The error limits for C_Q, η_Q, δ_σ, η_σ are ±0.02 MHz, ±0.03, ±5 ppm, ±0.10, respectively. The error limit for $J = {}^1J(^{17}O–^{187}Re)$ determined at the different temperatures is ±8 Hz while the error limits for D' and δ_J are much larger (~±100 Hz).

[b] The $J = {}^1J(^{17}O–^{187}Re)$ couplings reported for $KReO_4$ at temperatures above −90 °C and for NH_4ReO_4 at temperatures above −138 °C should not be considered the "true" ${}^1J(^{17}O–^{187}Re)$ coupling constants at the reported temperatures. The reason is that these data result from optimized fitting to the observed "doublet-like" line shapes (caused by dynamics) from variation of ${}^1J(^{17}O–^{187}Re)$ and D' ($^{17}O–^{187}Re) = D(^{17}O–^{187}Re) + \delta_J$. The "true" ${}^1J(^{17}O–^{187}Re)$ values for $KReO_4$ and NH_4ReO_4 are those shown at the temperatures of −90 and −138 °C, respectively (see text and figures).

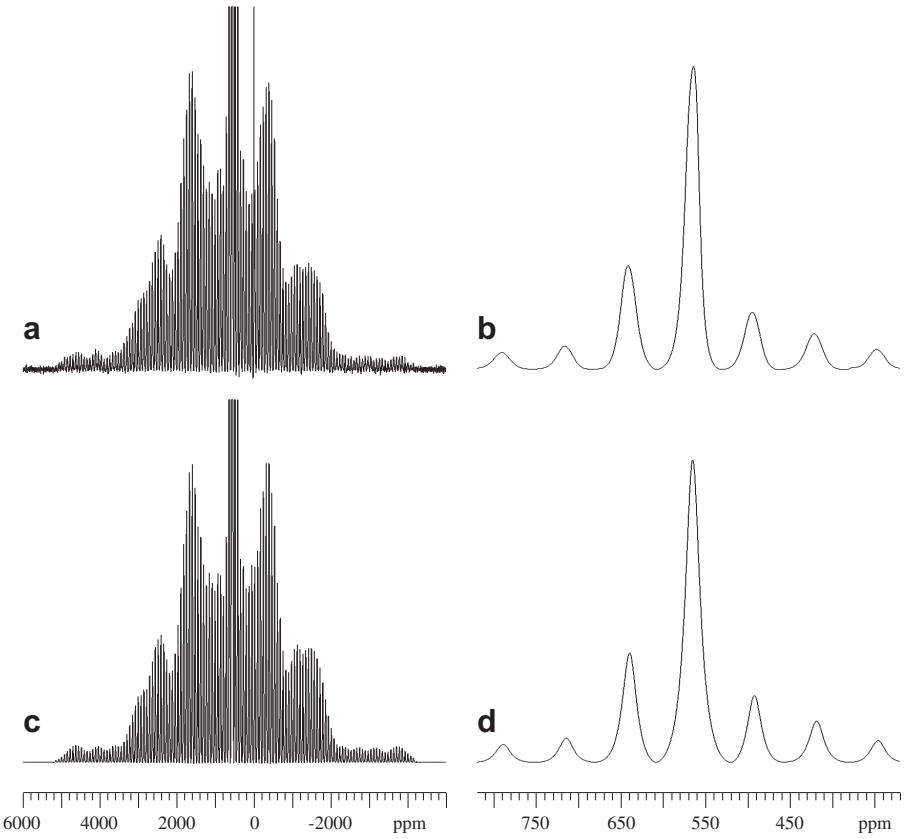

Fig. 3. 81.34 MHz (14.1 T) ^{17}O MAS NMR spectra of the ^{17}O-enriched sample of NH_4ReO_4, ν_r = 6000 Hz, and at RT (23 °C). (a) Experimental spectrum (5824 scans in 26 h) showing the complete manifold of spinning sidebands (ssbs) for a vertical expansion with a cut-off at 1/10 of the height for the centerband. As for $KReO_4$, please note that the resonance of unusual height at 0 ppm is caused by a minute amount of $H_2{}^{17}O$, which appears hard to completely remove from the sample immediately following its synthesis. (b) Horizontal expansion of the experimental spectrum in (a) for centerband region and a few of its ssbs, which illustrates the broadened ssbs without line shapes. (c and d) Fitted (XSTARS, $J = D = 0$, see text), simulated spectra corresponding to the spectra in (a and b). The optimized XSTARS parameters are listed in Tables 1a and 1b for $\Delta\theta$ = 0.000°.

due to the higher field of 21.1 T. Analysis of these spectra using XSTARS results in values for the spectral parameters, which all are within the error limits listed for the 14.1 T RT spectra of $KReO_4$ and NH_4ReO_4 in the two upper rows of Tables 1a and 1b. Similarly, the low-temperature 21.1 T ^{17}O MAS spectra for both $KReO_4$ and NH_4ReO_4 show almost identical appearances for the envelope of the ssb manifold for the STs as observed at RT. However, the resolution of the line shapes for the CT in particular, but also for the ssbs, increase with decreasing temperature for the spectra of both $KReO_4$ and NH_4ReO_4, with a higher resolution observed for $KReO_4$ at each fixed temperature, as also observed at RT. The results of the spectral analysis (XSTARS) for the spectra of $KReO_4$ and NH_4ReO_4 obtained at three different low temperatures (incl. the lowest temperatures) are listed in Tables 1a and 1b. They show that C_Q and δ_σ increase only slightly at lower temperatures, whereas the isotropic J coupling increases with the increased resolution observed for decreasing temperatures. Thus, for the above reasons only the ^{17}O MAS spectra obtained at the lowest temperatures for $KReO_4$ and NH_4ReO_4 (−90 °C and −138 °C, respectively) are shown below.

3.5. $KReO_4$

From the strong degradation in the S/N ratios of the ^{17}O MAS NMR spectra obtained at different temperatures on cooling the sample of $KReO_4$ down to the lowest temperature (−90 °C) for this sample and using identical experimental conditions (flip angle, relaxation delay, and number of scans) as for the RT spectrum, it became clear that the $T_1(^{17}O)$ relaxation time increases dramatically with decreasing temperature. Most importantly, it is observed that the width of the tilted, "doublet-like" line shape for the CT centerband (see e.g., Fig. 1b) and its ssbs increases with decreasing temperatures. Finally, at the temperature of −90 °C the complete experimental spectrum is shown in Fig. 4a with a relative cut-off height at 1/6 of the centerband height. At this temperature the maximum width observed for the unresolved centerband multiplet (∼1550 Hz) resolves into a six-line multiplet caused by isotropic J-coupling to the spin $I = 5/2$ ^{187}Re (^{185}Re) isotope, $J(^{17}O–^{187}Re) = -267$ Hz, as illustrated by the expansion shown in Fig. 4b for the central part of the full spectrum (Fig. 4a) and the expansion for the centerband in Fig. 4c. The result of an optimized fit (XSTARS) to the complete experimental spectrum (CT and STs) obtained at −90 °C is shown in Fig. 4d–f below the corresponding experimental spectra, while the resulting optimized spectral parameters are summarized in the fifth row of Tables 1a and 1b. Because of the estimated extremely long $T_1(^{17}O)$ relaxation time for $KReO_4$ (*vide supra*), and therefore long spectrometer time (∼7.5 h) required to achieve the decent S/N ratio for the spectrum in Fig. 4a, no additional low-temperature ^{17}O MAS experiments, such as determination of $T_1(^{17}O)$, $T_2(^{17}O)$, or $T_1(^{187}Re)$, have been attempted for this sample.

3.6. NH_4ReO_4

Following a few initial low-temperature ^{17}O MAS NMR experiments for the sample of NH_4ReO_4 it became clear, that $T_1(^{17}O)$

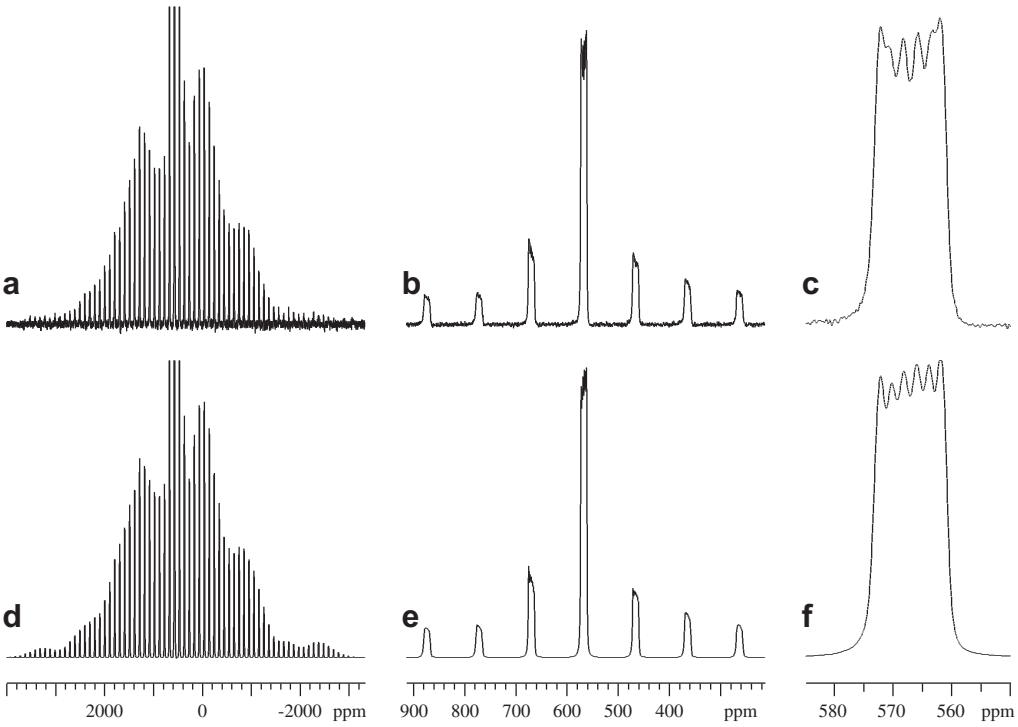

Fig. 4. 121.50 MHz (21.1 T) ^{17}O MAS NMR spectra of the ^{17}O-enriched sample of $KReO_4$, ν_r = 12401 Hz, and at −90 °C. (a) Experimental spectrum (512 scans in 4.5 h) showing the complete manifold of ssbs for a vertical expansion with a cut-off at 1/6 of the height for the centerband. We note that the resonance at 0 ppm in Fig. 1a, caused by the initially minute amount of $H_2{}^{17}O$ in the sample, has disappeared following a period of approximately 1 year after the preparation of the sample. Since the crystal structure [6] show $KReO_4$ is anhydrous and non-hygroscopic, we assume this is caused by evaporation and not by exchange of water. (b and c) Horizontal expansions of the complete experimental spectrum in (a). (b) Shows the centerband region and a few of its ssbs, and (c) an expansion of the centerband itself. The expansions in (b and c) clearly illustrate the increased resolution observed for these resonances in the spectrum of $KReO_4$ at −90 °C. (d–f) Fitted (XSTARS), simulated spectra corresponding to the experimental spectra in (a–c). The optimized XSTARS parameters are listed in Tables 1a and 1b, and for a deviation from exact magic-angle setting of $\Delta\theta = -0.059°$.

for NH_4ReO_4 (not determined) is very much shorter compared to that for $KReO_4$. Thus, by reducing the relaxation delay to 10 s and the number of scans to between 50 and 160, the S/N ratio for the NH_4ReO_4 sample improved significantly as compared to that observed for the spectra of $KReO_4$ (e.g., Fig. 4a). Within the allocated spectrometer time for our experiments, this allowed a large number of low- and also some high-temperature experiments to be performed for NH_4ReO_4, in order to characterize the type of dynamics causing the differences between the appearances of the ^{17}O RT MAS NMR spectra for $KReO_4$ and NH_4ReO_4.

On cooling the sample of NH_4ReO_4 to a temperature of −18 °C the centerband in the ^{17}O MAS spectrum starts splitting into a tilted, "doublet-like" line shape with a similar appearance to that observed for the centerband in the 14.1 T RT spectrum of $KReO_4$ shown in Fig. 1b. This line shape for NH_4ReO_4 allows extraction of an averaged value for $J(^{17}O–^{187}Re) \sim -218$ Hz and spectral parameters within error limits to those determined from its 14.1 T RT spectrum (Table 1a). Similar to the observation made for $KReO_4$, further cooling of the NH_4ReO_4 sample results in an increase of the width and improved resolution of the doublet-splitting for the CT centerband; the spectral parameters resulting from optimization to two such spectra obtained at temperatures of −59 °C and −90 °C are listed in Tables 1a and 1b (rows 6 and 7, respectively). Finally, at the temperature of −138 °C the CT centerbands resolve into six-line multiplets caused by $J(^{17}O–^{187}Re) = -278$ Hz, similar to the observation made for $KReO_4$ at −90 °C, however, at a much lower temperature for the NH_4^+ salt. The complete experimental spectrum is shown in Fig. 5a following a vertical expansion with a cut-off height at 1/6 for the centerband of its maximum height. A horizontal expansion for the central region of the experimental spectrum is displayed in Fig. 5b, while an expansion for the centerband is illustrated in Fig. 5c. The simulated spectrum resulting from an optimized fit to the full experimental spectrum in Fig. 5a is shown in Fig. 5d, while expansions of this simulated spectrum are shown in Fig. 5e and f below the corresponding expansions for the experimental spectrum. The optimized spectral parameters determined for NH_4ReO_4 at −138 °C are summarized in Tables 1a and 1b (row 8).

Following these low-temperature ^{17}O MAS experiments, it was tempting to perform a few high-temperature experiments for NH_4ReO_4 up to a maximum temperature of 70 °C. This temperature is about the upper limit for this NHMFL 21.1 T VT MAS probe, considering the expansion of the plastic materials used in the design/construction of its 3.2 mm stator. Starting out directly at the upper limit of 70 °C, the ^{17}O MAS NMR spectrum of NH_4ReO_4 appears as a single resonance (FWHM ∼ 2450 Hz) at the position for the CT and with no appearance of any ssbs for the STs at this temperature. By lowering the sample temperature to 46 °C, the manifold of ssbs for the STs starts to show-up again, however, with quite large line widths for the ssbs (∼5000 Hz). Finally, back to a temperature of 23 °C (RT), the spectrum appears similar to the very first RT spectrum obtained at 21.1 T. A high-temperature behavior similar to that seen for NH_4ReO_4 could not be observed for $KReO_4$ within the maximum upper temperature limit of 70 °C for the VT probe, but seems quite likely at temperatures above 70 °C.

In addition to the low-temperature ^{17}O MAS NMR experiments described above for NH_4ReO_4, a series of ^{17}O EXSY experiments, described in Section 2, have been performed at several temperatures in order to get a handle on the range of the corresponding $T_1(^{187}Re)$ values, and thereby, hopefully, also on the mechanism for the dynamics of the appearance/disappearance of the scalar $J(^{17}O–^{187}Re)$-coupling six-line multiplet patterns in the spectra at low temperatures. Furthermore, two standard $T_2(^{17}O)$ spin-echo experiments with rotor synchronization of the two inter pulse

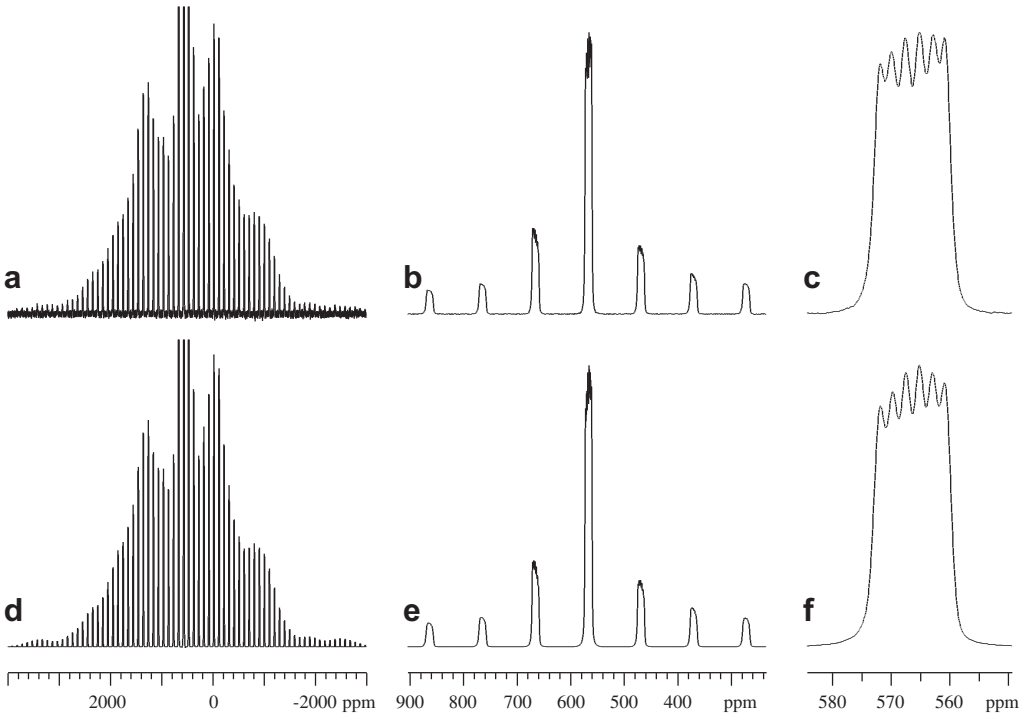

Fig. 5. 121.50 MHz (21.1 T) ^{17}O MAS NMR spectra of the ^{17}O-enriched sample of NH_4ReO_4, ν_r = 12000 Hz, and at −138 °C. (a) Experimental spectrum (160 scans in 0.5 h) showing the complete manifold of ssbs for a vertical expansion with a cut-off at 1/6 of the height for the centerband. It is noted that the resonance at 0 ppm in Fig. 3a, caused by the initially minute amount of $H_2{}^{17}O$ in the sample, has disappeared following a period of approximately 1 year after the preparation of the sample (we assume by evaporation; see note for $KReO_4$ in Fig. 4 which also holds for NH_4ReO_4). (b and c) Horizontal expansions of the complete experimental spectrum in (a). (b) Shows the centerband region and a few of its ssbs, and (c) an expansion of the centerband itself. The expansions in (b and c) clearly illustrate the increased resolution observed for these resonances in the spectrum of NH_4ReO_4 at −138 °C. (d–f) Fitted (XSTARS), simulated spectra corresponding to the experimental spectra in (a–c). The optimized XSTARS parameters are listed in Tables 1a and 1b, and for a deviation from exact magic-angle setting of $\Delta\theta$ = 0.045°.

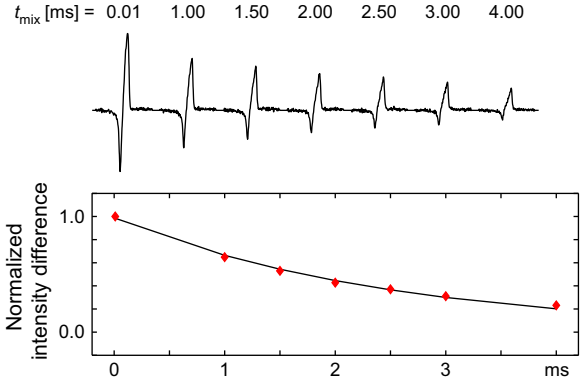

Fig. 6. $T_1(^{187}Re)$ determination for NH_4ReO_4 at −114 °C employing the indirect-detection ^{17}O EXSY experiment described above in Section 2. (Upper part) ^{17}O Antiphase-doublet MAS spectra of the centerband showing the decay of the doublet for increasing t_{mix} values. (Lower part) Shows the optimized exponential fit obtained for the normalized intensity difference for the antiphase doublets as a function of t_{mix} and resulting in a value $T_1(^{187}Re)$ = 2.5 ms at −114 °C (Table 2).

Table 2
Upper two rows: ^{187}Re spin–lattice times $T_1(^{187}Re)$ determined for NH_4ReO_4 via ^{17}O MAS NMR detection, using the EXSY experiment (see Section 2) at low temperatures. Lower two rows: Approximate ^{17}O spin–spin relaxation times $T_2(^{17}O)$ obtained at two widely different temperatures from three-point optimized fits to the respective spectral intensities.

$T_1(^{187}Re)$[a]	ms	4.3	2.5	2.0	1.4	0.5
Temp.	°C	−127	−114	−106	−98	−66
$T_2(^{17}O)$[b]	ms	1.0	0.8			
Temp.	°C	−98	−18			

[a] Error limits for the $T_1(^{187}Re)$ spin–lattice relaxation times are estimated to be within ±0.3 ms.
[b] Error limits for the $T_2(^{17}O)$ spin–spin relaxation times, determined from three-point optimized fits to the intensities for the two experimental spectra, are estimated to be within about ±0.1 ms.

delays were also performed for the NH_4ReO_4 sample at two quite different low temperatures to throw further light on the dynamics of the above experiments. The $T_1(^{187}Re)$ spin–lattice relaxation times for NH_4ReO_4, indirectly detected by ^{17}O MAS NMR, were determined in the temperature range from −127 °C and upwards until the ^{17}O signal became too weak at temperatures higher than −66 °C, thereby resulting in spectra from which $T_1(^{187}Re)$ could not be determined. As an example, Fig. 6 shows the appearance of the spectra obtained at the temperature of −114 °C for different mixing times, t_{mix}, and used for the extraction of $T_1(^{187}Re)$ at this temperature. The $T_1(^{187}Re)$ values determined by this method within the temperature range from −127 to −66 °C are summarized in Table 2. To our knowledge these are the first $T_1(^{187}Re)$ data reported for a perrhenate which, as mentioned (*vide supra*) in Section 1, are difficult to measure directly from the observed extremely broad static $^{185/187}Re$ powder spectra [12,14]. However, the reported recycles delays of 50 and 100 ms used in these studies [12,14] are consistent with our $T_1(^{187}Re)$ values determined here (Table 2). As pointed out in the following Section 4, the $T_1(^{187}Re)$ data are indicative of ^{17}O–^{187}Re self-decoupling [48,49] being responsible for the appearance/disappearance of the $J(^{17}O–^{187}Re)$ splittings in our spectra. Finally, two $T_2(^{17}O)$ spin-echo experiments were performed at temperatures of −98 and −18 °C, however, each for only three different spin-echo delay times of 2, 8, and 16 total rotor periods, respectively, to obtain an estimate for

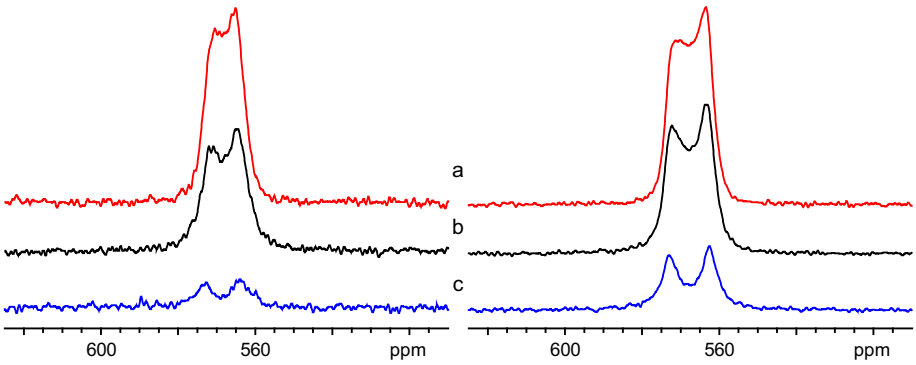

Fig. 7. $T_2(^{17}O)$ spin-echo experiments for NH_4ReO_4 performed at the two temperatures of −18 °C (left) and −98 °C (right) employing total rotor periods of (a) 2, (b) 8, and (c) 16 for the spin-echo time. The estimates for $T_2(^{17}O)$ at these temperatures, resulting from the two three-parameter exponential fits, are shown in Table 2.

the influence of $T_2(^{17}O)$ on the experiments with an increase in temperature. The outcome of these experiments are illustrated in Fig. 7, and the $T_2(^{17}O)$ values obtained from three-point fits of the intensities at −98 and −18 °C in Fig. 7 are 1.0 and 0.8 ms, respectively (Table 2).

4. Discussion

While the initial ^{17}O MAS NMR spectra for $KReO_4$ and NH_4ReO_4 obtained at 14.1 T and RT allow preliminary data to be determined for the indirect scalar $J(^{17}O–^{187}Re)$ and direct dipolar $D' = D + \delta_J$ spin–spin couplings in $KReO_4$ only, low-temperature ^{17}O MAS experiments are necessary to fully resolve the six-line multiplet patterns in the spectrum of NH_4ReO_4, but also for $KReO_4$, and preferably at high magnetic field to reduce the dipolar–quadrupolar broadening. For NH_4ReO_4 the resolution of this multiplet pattern requires the lowest achievable sample temperature (−138 °C) for the probe with the present condition of a spinning frequency $\nu_r = 12$ kHz, whereas for $KReO_4$ the six-line multiplet pattern becomes observable at the somewhat higher sample temperature of −90 °C (also for $\nu_r = 12$ kHz), and with no improvements in resolution at lower temperatures. At these low temperatures none of the spectra for the two perrhenates in Figs. 4c and 5c show any indication for the presence of two different oxygen sites in a 1:1 ratio. According to the crystal structures determined for $KReO_4$ [4,6] and NH_4ReO_4 [5,7,8] this could have been a possibility, since both crystal structures show the presence of two different tetrahedral sets of oxygen atoms around each of the K^+ and NH_4^+ cations with slightly different O–K and O–N distances for each of the two tetrahedral arrangements.

A closer look at the data summarized in Table 1a shows that the spectral parameters (i.e., quadrupole coupling (C_Q, η_Q), chemical shift (δ_{iso}, δ_σ, η_σ), and scalar $^1J(^{17}O–^{187}Re)$ coupling) are similar for $KReO_4$ and NH_4ReO_4 over the full temperature range studied, not at least when considering the error limits for these parameters. Moreover, with the exception of $^1J(^{17}O–^{187}Re)$, the temperature variations for these parameters generally fall within the error limits of the parameters, for the range of temperatures studied here. However, the gradually quite large increase in the apparent $^1J(^{17}O–^{187}Re)$ splitting from ~220 to ~280 Hz for both $KReO_4$ and NH_4ReO_4 across the temperature range (23 to −138 °C) should not be considered a "real" temperature dependence for the $^1J(^{17}O–^{187}Re)$ coupling constant. Instead we ascribe this effect to the experimentally observed increase in resolution/width of the tilted, "doublet-like" line shape for the centerband with a decrease in the sample temperature, caused by dynamic effects (self-decoupling of the six-line $^1J(^{17}O–^{187}Re)$ multiplet pattern, *vide infra*). Therefore, it is not surprising that optimized fitting to these experimental line shapes results in larger apparent $^1J(^{17}O–^{187}Re)$ splitting upon cooling until the two samples reach the low-temperatures (−90 and −138 °C, respectively), where the tilted, "doublet-like" line shapes obtain their maximum widths and split into six-line multiplets, and the *magnitudes* of $^1J(^{17}O–^{187}Re)$ become resolved with values in the range 270–280 Hz for the two compounds (Tables 1a and 1b).

Just as importantly, simulations show that the line shapes of the ssbs depend on the *relative* sign of $^1J(^{17}O–^{187}Re)$ and $D'(^{17}O–^{187}Re)$, i.e., if the two parameters have the same sign the shape of a given ssb is close to the mirror image to that observed for opposite signs. To understand this unexpected effect, which is unique for the ReO_4^- ions studied here, the factors governing the appearances of the ssbs must be considered. Generally three factors are important for the appearances of the ssb line shapes: (*i*) the relative positions of the six components corresponding to the six ^{187}Re eigenstates ($m_z(^{187}Re) = 5/2,\ 3/2,\ 1/2,\ -1/2,\ -3/2,\ -5/2$); (*ii*) the line shape caused by second-order ^{17}O quadrupole interaction; (*iii*) the intensity distribution (specific for each $m_z(^{187}Re)$ manifold) across the manifold of ssbs caused by the combined effect of the ^{17}O CSA and $D'(^{17}O–^{187}Re)$. The relative positions are predominantly determined by the isotropic J coupling and the second-order cross-term for the $D'(^{17}O–^{187}Re)$ and $C_Q(^{187}Re)$ interaction, which is proportional to $(1 - 3\cos^2\beta)\, D'(^{17}O–^{187}Re)\, C_Q(^{187}Re)$, where β is the angle between the two z-axes of the PAS systems for the $D'(^{17}O–^{187}Re)$ and $C_Q(^{187}Re)$ interaction. For the ReO_4^- ion β is close to the magic angle and the six manifolds are therefore approximately evenly spaced by the isotropic J coupling. The ^{17}O quadrupole coupling $C_Q(^{17}O) \sim 1.3$ MHz (Table 1a) is too small to contribute significantly to the line shape and therefore each ssb is composed of six almost evenly spaced Lorentzian/Gaussian lines with different amplitudes. The changes in the ssb line shapes observed in the ^{17}O MAS spectrum is therefore almost exclusively given by the combined first-order ^{17}O CSA and $D'(^{17}O–^{187}Re)$ interaction. For coincident PAS for the two interactions, which is nearly fulfilled for the ReO_4^- ion (Table 1a), and an asymmetry parameter $\eta_\sigma = 0$ the combined effect is similar to a CSA effect given by $\delta_\sigma + m_z(^{187}Re)\, D'(^{17}O–^{187}Re)$. If the sign of the isotropic J coupling is changed, the positions of the two manifolds $m_z(^{187}Re) = \pm m$, $m = 5/2,\ 3/2,\ 1/2$ are interchanged and the line shape of each ssb changes into its mirror image. If the sign of $D'(^{17}O–^{187}Re)$ is changed it is seen that the effective CSA also changes with the sign of $m_z(^{187}Re)$. Thus, only the relative sign of $^1J(^{17}O–^{187}Re)$ and $D'(^{17}O–^{187}Re)$ is important for the line shapes of the ssbs. All optimized fits to the experimental line shapes for the ssbs of the STs and CT show that $^1J(^{17}O–^{187}Re)$ and $D'(^{17}O–^{187}Re)$ have the same sign, as e.g. observed from the spectra of $KReO_4$ in Figs. 1b, e, 2a, b, and 4b, e,

and for NH_4ReO_4 in Fig. 5b and e. In contrast, for opposite signs of $^1J(^{17}O–^{187}Re)$ and $D'(^{17}O–^{187}Re)$ simulations result in mirror images of the tilted, "doublet-like" line shape for the CT centerband and for the line shape of each indivual ssb for the STs throughout the complete spectrum, compared to those shown in the experimental and simulated spectra mentioned above and as predicted. Thus, with reference to Eq. (15) below and the usual assumption that the magnitude of the anisotropy (δ_J) for the isotropic $^1J(^{17}O–^{187}Re)$ coupling has a lower value than the calculated direct dipolar coupling $D(^{17}O–^{187}Re)$ (Eq. (16)), which is negative ($\gamma_I < 0$ and $\gamma_S > 0$), we can conclude that $^1J(^{17}O–^{187}Re)$ and $D'(^{17}O–^{187}Re)$ are both negative.

In addition to the error limits discussed above with special relation to the values determined for $^1J(^{17}O–^{187}Re)$, we emphasize that in contrast to the scalar $^1J(^{17}O–^{187}Re)$ couplings, the D' values determined from the optimized fit of the spectra and reported in Table 1a are associated with substantial error limits of at least ~±100 Hz. Anyway, for the range of $D'(^{17}O–^{187}Re)$ values determined and listed in Table 1a, we found it of interest to derive estimates for the anisotropies (δ_J) of the isotropic $^1J(^{17}O–^{187}Re)$ couplings, according to the definition, see Section 2

$$D'(^{17}O - {}^{187}Re) = D(^{17}O - {}^{187}Re) + \delta_J \quad (15)$$

This requires calculation of the direct dipolar $^{17}O–^{187}Re$ spin–spin coupling

$$D(^{17}O - {}^{187}Re) = (\gamma_I\gamma_S\mu_0\hbar)(8\pi^2 r_{IS}^3)^{-1}, \quad (16)$$

where $I = {}^{17}O$ and $S = {}^{187}Re$, which again requires a good knowledge for the $r(^{17}O–^{187}Re)$ bond lengths at RT and ~−100 °C. From the many crystal structures determined for $KReO_4$ and NH_4ReO_4 at RT and low temperatures [4–8], we have evaluated the following average bond lengths $r(^{17}O–^{187}Re)$ = 1.729 and 1.735 Å, at temperatures of 22 and −100 °C, respectively, for both compounds. Thus, substituting these values into Eq. (16) we obtain $D(^{17}O–^{187}Re)$ = −726 and −697 Hz at 22 and −100 °C, respectively, to be used for calculations of the estimates for δ_J. Thus, even considering the large error limits for $D'(^{17}O–^{187}Re)$ and quite good precisions for the two calculated $D(^{17}O–^{187}Re)$ dipolar couplings (Eq. (16)) from literature bond lengths at different temperatures, it is believed that the J anisotropoies (δ_J) listed in Table 1a are significant, however, with some quite large error limits.

To further explore the nature of the mechanism for the full and clear appearances of the J-coupling splittings in the low-temperature ^{17}O MAS spectra for $KReO_4$ and NH_4ReO_4 at −90 and −138 °C, respectively, a series of the ^{17}O EXSY experiments described above, were performed for NH_4ReO_4 to probe values for $T_1(^{187}Re)$ in the temperature range −127 to −66 °C (Fig. 6) and led to the results summarized in the upper part of Table 2. Most interestingly, these data fall in the range (4.3–0.5 ms), where self-decoupling of the $^1J(^{17}O–^{187}Re)$ splittings caused by $T_1(^{187}Re)$ spin–lattice relaxation rates are expected to occur. From the magnitude $|^1J(^{17}O–^{187}Re)|$ = 278 Hz (Table 1a), determined from the fully resolved J-coupling pattern at −138 °C in Fig. 5c, we find that the disappearance of the individual J splittings by self-decoupling requires $T_1(^{187}Re)$ to be $< 1/|^1J(^{17}O–^{187}Re)| = 1/278 = 3.6$ ms [48]. This value is in excellent agreement with the results obtained from exponential fits of the difference in intensities for the ^{17}O EXSY type experiments at the different temperatures (e.g., Fig. 6), which are summarized in Table 2. For the "doublet-like" line shape observed for the centerband at temperatures from ~−115 °C and up to ~−18 °C, $T_1(^{187}Re)$ is required to be $<(5\,^1J(^{17}O–^{187}Re))^{-1}$, i.e., <0.7 ms for the "doublet-like" line shape starting to collapse into a singlet as observed above ~−18 °C, e.g., at RT (23 °C) for NH_4ReO_4 (Fig 3b). We note that upon cooling the NH_4ReO_4 sample, an indication for the appearance of a "doublet-like" line shape within the centerband is observed at the first temperature-stop of −2 °C. Unfortunately, at temperatures higher than ~−70 °C the S/N level for the EXSY experiment has degraded to a level that makes determination of reliable $T_1(^{187}Re)$ data meaningless. Since this decrease in S/N could be caused by a decrease in $T_2(^{17}O)$ with increasing temperature, it was decided to test this suspicion by performing standard ^{17}O spin-echo $T_2(^{17}O)$ experiments at the two temperatures of −98 °C and −18 °C and for ν_r = 12.0 kHz. The results of these two experiments, each employing only three different total spin-echo periods of 2, 8, and 16 rotor periods, i.e., corresponding to total spin-echo times of 166, 666, and 1333 μs, respectively, are illustrated in Fig. 7. The corresponding estimates for $T_2(^{17}O)$, obtained from three-point exponential fits to the intensities for the two sets of spectra, are shown in the lower part of Table 2. From the minor decrease for T_2 (^{17}O) (1.0 → 0.8 ms) observed by increasing the temperature from −98 to −18 °C, we conclude that $T_2(^{17}O)$ is clearly *not* the reason for causing a S/N limit for determination of $T_1(^{187}Re)$ data at temperatures above ~−70 °C. From the temperature dependence of $T_1(^{187}Re)$ observed from the data in Table 2, we expect a continuous decrease in $T_1(^{187}Re)$ below the value of 0.5 ms for temperatures above −66 °C due to increasing reorientational motion of the NH_4^+ (and ReO_4^-) ions (*vide infra*). These low $T_1(^{187}Re)$ values make the "doublet-like" $^1J(^{17}O–^{187}Re)$ splittings starting to collapse such that the three-pulse EXSY experiment is unable to create the antiphase coherence necessary for the $T_1(^{187}Re)$ measurements. It is interesting to note that several early low-temperature NQR studies on NH_4ReO_4 have observed a "wipeout region" of the NQR frequencies in the temperature range of about −110 to −50 °C [11,13]. This temperature range is very much identical to the region where the ^{17}O S/N for the EXSY experiment suddenly decreases to a level that excludes determination of $T_1(^{187}Re)$. It has been proposed and shown [13] that this "wipeout region" for NH_4ReO_4 is caused by either temperature- or pressure-gradients across the sample. From the temperature calibration experiments using $Pb(NO_3)_2$ (see Section 2), we know that our sample is exposed to temperature gradients at both low- and high-temperatures within the MAS probe and therefore is susceptible to the same effects as observed for the NQR "wipeout region" experiments. From the $T_1(^{187}Re)$ experiments performed in the temperature range −127 to −66 °C (Table 2) we conclude that self-decoupling is the mechanism responsible for the appearance/disappearance of the six-line multiplet, $^1J(^{17}O–^{187}Re)$-coupling pattern in the temperature range −138 °C to −115 °C, and that this mechanism combined with very short $T_1(^{187}Re)$ relaxation times account for the gradual collapse of the "doublet-like" line shape in the temperature range −115 °C to −18 °C.

For temperatures higher than 23 °C (RT) the ^{17}O centerband and ssbs for the STs in the MAS spectrum of NH_4ReO_4 start broadening, and when the centerband reaches a FWHM = 2450 Hz at 70 °C, the complete ^{17}O ssb pattern has disappeared and partly merged into the ^{17}O centerband. Unfortunately, the plastic materials, used for the stator design of the MAS probe, do not allow for a follow-up of the molecular dynamics for NH_4ReO_4 at higher temperatures. However, upon cooling to a temperature of 46 °C, the ssbs for the STs start to reappear with a FWHM = 5000 Hz and finally return to the normal RT appearance for the ^{17}O MAS spectrum at 23 °C. These observations show that at a temperature of 70 °C, the molecular reorientational dynamics for the NH_4^+ ions in NH_4ReO_4 [13], and simultaneously most likely also for the ReO_4^- ions, have increased to a point, which causes the complete ssb pattern for the STs to disappear. From the approximate width of the ssb pattern (~430 kHz) at 21.1 and 14.1 T, it is estimated that the reorientational correlation times for these ions would be on the order of 2×10^{-6} s.

As pointed out in Section 1, several $^1J(^{17}O\text{-}M)$ coupling constants, where M is a quadrupolar nucleus (M = ^{51}V, ^{53}Cr, ^{55}Mn,

Table 3
One-bond isotropic $^1J(^{17}O–M)$ couplings and the corresponding reduced spin–spin coupling constants, $^1K(^{17}O–M)$, where M is a quadrupolar nucleus (M = ^{51}V, ^{53}Cr, ^{55}Mn, ^{95}Mo, ^{99}Tc, and ^{187}Re) and a spin-1/2 nucleus (M = ^{13}C), have been used to illustrate correlations between $^1K(^{17}O–M)$ and the atomic number M (see text).

Spin isotope M	^{13}C	^{51}V	^{53}Cr	^{55}Mn	^{95}Mo	^{99}Tc	^{187}Re
Atomic no. of M	6	23	24	25	42	43	75
$^1J(^{17}O–M)$[f]	25.0[a]	−62[b]	10[b]	−29.6[b]	40.4[b,c]	−131.6[d]	−278[e]
$^1K(^{17}O–M)$[g]	−6.1	14.4	10.9	7.3	37.9	35.7	74.0

[a] From Ref. [28], where $^1J(^{17}O–^{13}C)$ is the average of the two experimentally determined values of +24.7 and +25.3 Hz for glycine, and the positive sign follows from the CASTEP calculated average value for $^1K(^{17}O–^{13}C) = -6.4 \times 10^{20}$ NA^{-2} m^{-3} [28].
[b] From Ref. [33], where some of the values are the average of two independent determinations and the signs follow from the correlation shown in Fig. 8 and the present text.
[c] From Ref. [32].
[d] From Ref. [34].
[e] Value for NH_4ReO_4 determined in this work.
[f] ^1J couplings in Hz.
[g] Reduced ^1J couplings ^1K in 10^{20} NA^{-2} m^{-3} and calculated from the ^1J values shown in the row for $^1J(^{17}O–M)$.

^{95}Mo, and ^{99}Tc), have been determined from solution-state NMR [32–34]. Moreover, two of these studies [33,34] proposed linear correlations between the corresponding *reduced* coupling constants, $^1K(^{17}O–M) = (2\pi\ ^1J(^{17}O–M))/(\gamma_{17O}\ \gamma_M\ \hbar)$, and the atomic number for M, but apparently with opposite sign for the slopes of the correlations (*vide infra*). The most recent study [34] called for a possible extension of the correlation using yet higher M-atomic number for $^1J(^{17}O–M)$, e.g., M = $^{185/187}Re$ or ^{183}W for the ReO_4^- or WO_4^{2-} ions (*vide supra*). The present result for $^1J(^{17}O–^{187}Re) = -268$ and -278 Hz for $KReO_4$ and NH_4ReO_4, respectively, allow for such an extension. The data, including both $^1J(^{17}O–M)$ and $^1K(^{17}O–M)$ for all elements M determined so far, even for the recently determined two $^1J(^{17}O–^{13}C)$ values in glycine and their sign from DFT CASTEP calculations [28], are summarized in Table 3. With the exception of the negative sign determined for $^1J(^{17}O–^{187}Re)$ in ReO_4^- from the present study, no sign have to our knowledge been determined for the $^1J(^{17}O–M)$ coupling constants where M is a quadrupolar nucleus. However, following the positive sign for the reduced coupling constant $^1K(^{17}O–^{187}Re)$ in ReO_4^-, it is tempting to assume a positive sign for $^1K(^{17}O–M)$ for the other quadrupolar nuclei as done in Table 3. A plot of the $^1K(^{17}O–M)$ values for the six quadrupolar nuclei in Table 3 versus their atomic number M is shown in Fig. 8 along with a solid line resulting from a linear regression analysis for these six points. Despite being a spin-1/2 nucleus, the value of $^1K(^{17}O–^{13}C)$ for M = ^{13}C (atomic number 6) has followingly been introduced as the point in red in Fig. 8. It is very encouraging to observe how well these recent data in both magnitude and sign for $^1J(^{17}O–^{13}C)/^1K(^{17}O–^{13}C)$ [28] fit into the linear correlation shown in Fig. 8, which clearly support our assumption of a positive sign for all reduced $^1K(^{17}O–M)$ couplings. Another interesting feature, which appears from the plot in Fig. 8, is the apparent linear correlations for the three group V, VI, and VII elements of ^{51}V, ^{53}Cr, and ^{55}Mn in VO_4^{3-}, CrO_4^{2-}, and MnO_4^- noted earlier by Lutz et al. [33], and similarly for the two higher group VI and VII elements of ^{95}Mo and ^{99}Tc in MoO_4^{2-} and TcO_4^-. The apparent linear correlation for the ^{51}V, ^{53}Cr, and ^{55}Mn oxoanions in Fig. 8 is very much parallel to a line through the points for ^{95}Mo and ^{99}Tc, however, most interestingly with the lighter element (^{51}V and ^{95}Mo, respectively) exhibiting the largest $^1K(^{17}O–M)$ values for the two groups in both cases. The negative slope for the apparent correlations observed for these two groups is clearly opposite to the positive slope obtained for the correlation of $^1K(^{17}O–M)$ with increasing M-atomic number as has now been established in Fig. 8 and called for earlier [34]. These correlations seem worth exploring in future experimental and theoretical studies.

Finally, despite the very different disordered crystal structure for the ReS_4^- anion, investigated recently by solid-state ^{33}S MAS and static NMR [3], compared to the crystal structures for the two ReO_4^- anion structures studied in this work by ^{17}O MAS NMR, it is tempting to compare the ^{33}S and ^{17}O solid-state quadrupole and chemical shift data resulting from the two studies. We note that $C_Q(^{33}S)$ for ReS_4^- is a factor ~2 *higher* compared to $C_Q(^{17}O)$ for ReO_4^-, which is quite similar to the factor found from a comparison of $C_Q(^{33}S)$ and $C_Q(^{17}O)$ for the tetrathio and tetraoxoanions WX_4^{2-} (X = S, O) in identical crystal structures, as recently reported [1]. In contrast, it is noted that the $\delta_\sigma(^{33}S)$ values for ReS_4^- is a factor ~2 *lower* compared to the $\delta_\sigma(^{17}O)$ values for the ReO_4^- anions reported here, and also compared to the corresponding δ_σ values reported recently for WS_4^{2-} and WO_4^{2-} [1].

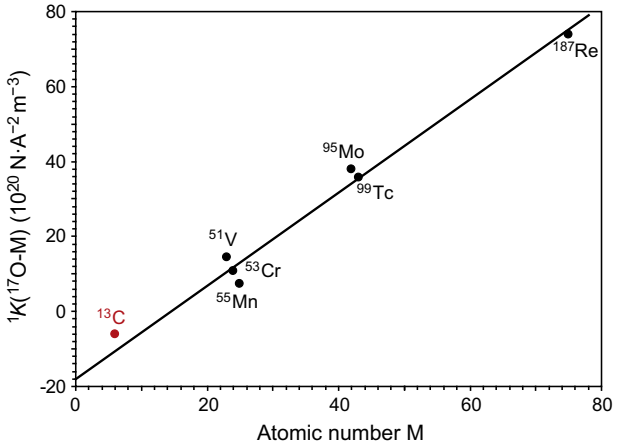

Fig. 8. Plot of the reduced one-bond coupling constants $^1K(^{17}O–M)$ ($\times 10^{20}$ NA^{-2} m^{-3}) in Table 3 versus the atomic number for M (M = ^{51}V, ^{53}Cr, ^{55}Mn, ^{95}Mo, ^{99}Tc, and ^{187}Re) shown as black-filled circles. Linear regression analysis for these points results in the line $^1K(^{17}O–M) = 1.2401$ M -17.979 shown in the plot. The recently determined experimental value for $^1J(^{17}O–^{13}C)/^1K(^{17}O–^{13}C)$ in glycine along with its sign (from CASTEP calculations) [28] has been introduced as the red-filled circle in the plot, but has not been used in the linear regression analysis (see also the text and Table 3).

Acknowledgments

The use of the facilities at the Instrument Centre for Solid-State NMR Spectroscopy, Aarhus University, sponsored by two Danish Science Research Councils, Teknologistyrelsen, the Carlsberg Foundation, Direktør Ib Henriksens Foundation is acknowledged. A large portion of this work was performed at the National High Magnetic Field Laboratory, which is supported by National Science Foundation Cooperative Agreement No. DMR-0654118, the State of Florida, and the U.S. Department of Energy.

References

[1] H.J. Jakobsen, H. Bildsøe, J. Skibsted, M. Brorson, I. Hung, Z. Gan, Synthesis of ^{17}O-labeled Cs_2WO_4 and its ambient- and low-temperature solid-state ^{17}O MAS NMR spectra, Inorg. Chem. 50 (2011) 7676–7684.

[2] Ref. [1] and the list of references cited in its Ref. (1a–1e)

[3] H.J. Jakobsen, H. Bildsøe, J. Skibsted, M. Brorson, P. Gor'kov, Z. Gan, A strategy for acquisition and analysis of complex natural abundance ^{33}S solid-state NMR spectra of a disordered tetrathio transition-metal anion, J. Magn. Reson. 202 (2010) 173–179.

[4] C.J.L. Lock, G. Turner, A reinvestigation of the crystal structure of potassium perrhenate, Acta Cryst. B31 (1975) 1764–1765.

[5] G.J. Kruger, E.C. Reynhardt, Ammonium perrhenate at 295 and 135 K, Acta Cryst. B34 (1978) 259–261.

[6] R.J.C. Brown, B.M. Powell, S.N. Stuart, Thermal effects in the structure of potassium perrhenate, Acta Cryst. C49 (1993) 214–216.

[7] B.M. Powell, R.J.C. Brown, A.M.C. Harnden, J.K. Reid, Thermal effects in the structure of ammonium perrhenate, Acta Cryst. B49 (1993) 463–468.

[8] I.P. Swainson, R.J.C. Brown, Refinement of ammonium perrhenate structure using a pseudo-spin model for the ammonium ion orientation, Acta Cryst. B53 (1997) 76–81.

[9] M.T. Rogers, K.V.S. Rama Rao, Rhenium pure quadrupole resonance spectrum of potassium perrhenate, J. Chem. Phys. 49 (1968) 1229–1231.

[10] M.T. Rogers, K.V.S. Rama Rao, Pure quadrupole resonance spectra of perrhanates and periodates, J. Chem. Phys. 58 (1973) 3233–3235.

[11] R.A. Johnson, M.T. Rogers, Anomalous temperature dependence of the NQR frequency in NH_4ReO_4, J. Magn. Reson. 15 (1974) 584–589.

[12] C.M. Widdifield, A.D. Bain, D.L. Bryce, Definitive solid-state $^{187}/^{185}$Re NMR spectral evidence for and analysis of the origin of high-order quadrupole-induced effects for I = 5/2, Phys. Chem. Chem. Phys. 13 (2011) 12413–12420 and references cited therein.

[13] H.E. Petch, E.C. Reynhardt, A. Watton, Ammonium ion reorientation in NH_4ReO_4 by NMR, J. Magn. Reson. 29 (1978) 1–6.

[14] R.W. Schurko, S. Wi, L. Frydman, Dynamic effects on the powder line shapes of half-integer nuclei: a solid-state NMR study of XO_4^- groups, J. Chem. Phys. A 106 (2002) 51–62.

[15] A.C. Olivieri, L. Frydman, L.E. Diaz, A simple approach for relating molecular and structural information to the dipolar coupling ^{13}C–^{14}N in CPMAS NMR, J. Magn. Reson. 75 (1987) 50–62.

[16] A.C. Olivieri, L. Frydman, M. Grasselli, L.E. Diaz, Microcomputer simulation of solid-state NMR line shapes affected by quadrupolar nuclei, Magn. Reson. Chem. 26 (1988) 615–618.

[17] A.C. Olivieri, Quadrupolar effects in the CPMAS NMR spectra of spin-1/2 nuclei, J. Magn. Reson. 81 (1989) 201–205.

[18] R.K. Harris, A.C. Olivieri, Quadrupolar effects transferred to spin-1/2 magic-angle spinning spectra of solids, Prog. Nucl. Magn. Reson. Spectrosc. 24 (1992) 435–456.

[19] D. Massiot, F. Fayon, M. Deschamps, S. Cadars, P. Florian, V. Montouillout, N. Pellerin, J. Hiet, A. Rakhmatullin, C. Bessada, Detection and use of small *J* couplings in solid-state NMR experiments, Comput. Rendus Chim. 13 (2010) 117–129.

[20] F. Chen, G.M. Bernard, R.G. Cavell, R. McDonald, M.J. Ferguson, R.E. Wasylishen, Solid-state ^{115}In and ^{31}P NMR studies of triarylphosphine indium trihalide adducts, J. Am. Chem. Soc. 132 (2010) 5479–5493 and references cited therein.

[21] M.H. Frey, S.J. Opella, High-resolution features of the ^{13}C NMR spectra of solid amino acids and peptides, J. Chem. Soc., Chem. Commun. (1980) 474–475.

[22] C.J. Groombridge, R.K. Harris, K.J. Packer, B.J. Say, S.F. Tanner, High-resolution ^{13}C NMR spectra of solid nitrogen-containing compounds, J. Chem. Soc., Chem. Commun. (1980) 174–175.

[23] G. Wu, R.E. Wasylishen, The influence of the heteronuclear dipolar interaction on nuclear magnetic resonance spectra of quadrupolar nuclei, Mol. Phys. 95 (1998) 1177–1183.

[24] S. Wi, L. Frydman, Residual dipolar couplings between quadrupolar nuclei in high resolution solid state NMR: description and observations in the high-field limit, J. Chem. Phys. 112 (2000) 3248–3261.

[25] L. Frydman, J.S. Harwood, Isotropic spectra of half-integer quadrupolar spins from bidimensional magic-angle spinning NMR, J. Am. Chem. Soc. 117 (1995) 5367–5368.

[26] A. Llor, J. Virlet, Towards high-resolution NMR of more nuclei in solids: sample spinning with time-dependent spinner axis angle, Chem. Phys. Lett. 152 (1988) 248–253.

[27] A. Samoson, E. Lipmaa, A. Pines, High resolution solid-state NMR. Averaging of second-order effects by means of a double-rotor, Mol. Phys. 65 (1988) 1013–1018.

[28] I. Hung, A.C. Uldry, J. Becker-Baldus, A.L. Webber, A. Wong, M.E. Smith, S.A. Joyce, J.R. Yates, C.J. Packard, R. Dupree, S.P. Brown, Probing heteronuclear ^{15}N–^{17}O and ^{13}C–^{17}O connectivities and proximities by solid-state NMR spectroscopy, J. Am. Chem. Soc. 131 (2009) 1820–1834.

[29] F.A. Perras, D.L. Bryce, Residual dipolar coupling between quadrupolar nuclei under magic-angle spinning and double-rotation conditions, J. Magn. Reson. 213 (2011) 82–89.

[30] S. Wi, V. Frydman, L. Frydman, Residual dipolar couplings between quadrupolar nuclei in solid state nuclear magnetic resonance at arbitrary fields, J. Chem. Phys. 114 (2001) 8511–8519.

[31] D. Iuga, C. Morais, Z. Gan, D.R. Neuville, L. Cormier, D. Massiot, NMR heteronuclear correlation between quadrupolar nuclei in solids, J. Am. Chem. Soc. 127 (2005) 11540–11541.

[32] R.R. Vold, R.L. Vold, Nuclear relaxation and spin-spin coupling in aqueous sodium molybdate, J. Chem. Phys. 61 (1974) 4360–4361.

[33] O. Lutz, W. Nepple, A. Nolle, Indirect spin-spin-coupling between ^{17}O and other quadrupolar nuclei in oxyanions, Z. Naturforsch. 31a (1976) 1046–1050.

[34] M.J. Buckingham, G.E. Hawkes, J.R. Thornback, The ^{99}Tc and ^{17}O nuclear magnetic spectra of TcO_4^- – the first detailed report on a ^{99}Tc resonance, Inorg. Chim. Acta 56 (1981) L41–L42.

[35] S. Schramm, E. Oldfield, High-resolution oxygen-17 NMR of solids, J. Am. Chem. Soc. 106 (1984) 2502–2506.

[36] J. Bank, A. Schwenk, ^{183}Tungsten NMR studies, Z. Phys. B20 (1975) 75–80.

[37] H.J. Jakobsen, A.R. Hove, H. Bildsøe, J. Skibsted, Satellite transitions in natural abundance ^{33}S MAS NMR of alums – sign change with zero-crossing of C_Q in a variable-temperature study, J. Magn. Reson. 180 (2006) 170–177.

[38] H.J. Jakobsen, A.R. Hove, H. Bildsøe, J. Skibsted, M. Brorson, Long-term stability of rotor-controlled MAS frequencies to 0.1 Hz proved by ^{14}N MAS NMR experiments and simulations, J. Magn. Reson. 185 (2007) 159–163.

[39] T. Bjorholm, H.J. Jakobsen, ^{31}P MAS NMR of P_4S_3. Crystalline-to-plastic phase transition induced by MAS in a double air-bearing stator, J. Magn. Reson. 84 (1989) 204–211.

[40] A. Bielecki, D.P. Burum, Temperature dependence of ^{207}Pb MAS spectra of solid lead nitrate. An accurate, sensitive thermometer for variable-temperature MAS, J. Magn. Reson. A 116 (1995) 215–220.

[41] H.J. Jakobsen, High-speed MAS of quadrupolar nuclei in solids, in: D.M. Grant, R.K. Harris (Eds.), Encyclopedia of Nuclear Magnetic Resonance, vol. 4, Wiley, New York, 1995, pp. 2370–2379;
H.J. Jakobsen, V. Langer, P. Daugaard, H. Bildsøe, A device and method for magic-angle adjustment with millidegree accuracy using MAS of quadrupolar nuclei, 31st ENC, Asilomar, Poster WP 19, 1990.

[42] J. Jeener, B.H. Meier, P. Bachmann, R.R. Ernst, Investigation of exchange processes by two-dimensional NMR spectroscopy, J. Chem. Phys. 71 (1979) 4546–4553.

[43] M.G. Colombo, B.H. Meier, R.R. Ernst, Rotor-driven spin diffusion in natural-abundance ^{13}C spin systems, Chem. Phys. Lett. 146 (1988) 189–196.

[44] H.J. Jakobsen, J. Skibsted, H. Bildsøe, N.C. Nielsen, Magic-angle spinning NMR spectra of satellite transitions for quadrupolar nuclei in solids, J. Magn. Reson. 85 (1989) 173–180.

[45] J. Skibsted, N.C. Nielsen, H. Bildsøe, H.J. Jakobsen, Satellite transitions in MAS NMR spectra of quadrupolar nuclei, J. Magn. Reson. 95 (1991) 88–117.

[46] Varian Manual, STARS (SpecTrum Analysis for Rotating Solids) User's Guide, Publication No 87-195233-00, Rev. A0296, 1996.

[47] K. Eichele, R.E. Wasylishen, WSolids1: Solid-State NMR Spectrum Simulation Package, v. 1.19.11, University of Tubingen, Tubingen, Germany, 2009.

[48] Reference [18], section 3.6, page 446 on "Self-decoupling" and references cited therein.

[49] R.W. Schurko, R.E. Wasylishen, J.H. Nelson, Effect of cobalt-59 self-decoupling on the solid-state ^{31}P CP/MAS NMR spectra of cobaloximes, J. Phys. Chem. 100 (1996) 8057–8060.